NOVA SCHOOL OF SCIENCE & TECHNOLOGY

DEPARTAMENT OF LIFE SCIENCES

FILIPA VIVIANA ROCHA MARTINEZ OLIVEIRA

BSc in Biochemistry

ENDOTHELIAL CELL-SPECIFIC PHOSPHATASE VE-PTP IN REGULATION OF ENDOTHELIAL BIOLOGY

MASTER IN MOLECULAR GENETICS AND BIOMEDICINE

NOVA University Lisbon

November, 2021

NOVA SCHOOL OF SCIENCE & TECHNOLOGY

DEPARTAMENT OF LIFE SCIENCES

ENDOTHELIAL CELL-SPECIFIC PHOSPHATASE VE-PTP IN REGULATION OF ENDOTHELIAL BIOLOGY

FILIPA VIVIANA ROCHA MARTINEZ OLIVEIRA
BSc in Biochemistry

Adviser: Lena Claesson-Welsh, Professor, Uppsala University

Co-advisers: Alexandra Fernandes, Assistant Professor, NOVA School of Science and Technology

Examination Committee:

Chair: Dr. Margarida Casal Ribeiro Castro Caldas Braga, Assistant Professor, NOVA School of Science and Technology, NOVA University Lisbon

Rapporteurs: Dr. Sérgio Jerónimo Rodrigues Dias, Professor at Lisbon School of Medicine, Lisbon University

Members: Dr. Lena Claesson-Welsh, Professor at Uppsala University

MASTER IN MOLECULAR GENETICS AND BIOMEDICINE

NOVA University Lisbon
November, 2021

To my family

ACKNOWLEDGMENTS

Along my dissertation I had the opportunity to meet wonderful people who helped me through this journey. I would like to express my sincere gratitude to every one of you for always supporting me and for all the knowledge you shared with me.

I would like to thank Susan Quaggin for the mouse strain used in this study.

A special thanks to my supervisor Lena, for giving me the opportunity to work on her lab, and for all the help during this challenging project. I am very grateful for all advises, excellent feedback and knowledge you shared with me during our meetings. For always being so supportive, for the patience and encouragement especially when things were not working out. I have learn a lot about science and also I have grown a lot professionally thanks to you. I can never thank you enough for giving me this opportunity.

Next, I would like to thank my co-supervisor Alexandra for the support and for all the emails clarifying my many doubts.

A big thanks to my Swedish mums. Pernilla thank you for teaching me everything about cell culture, how to master a western blot and all the lab work when I first started. For always being there for my questions and for everything you do at the lab. Mimmi thank you for your patience when teaching me all about animal work and how to properly do an intraperitoneal injection in pups, and also for your contagious good energy and your kind words that always motivated me to do my best. I am forever grateful for all the support, troubleshooting discussions and expertise you shared with me.

I also need to thank Yi for making everything look easier, for your patience and time to answer my questions, to teach me all about retinas quantifications and for always helping me analysing data. For all the discussions, excellent advises, protocols and for laughing when sometimes something would not work, making me feel less stressed.

Many thanks to all the past and present lab members. Sagnik, thanks for many talks and for always be willing to help. Yindi and Elin for all the help and advises. Emmanuel, Mark, Sofia and Tor for contributing to a pleasant work environment. Miguel for teaching me how to mount slides and for the chats, and Dom for all the help, for the Swedish lessons and for being so funny.

I would also like to thank the rest of the VascBio community at Rudbeck that contributes to a nice work environment where it is easy to ask for help and advice.

Finally, I would like to thank my family, my lovely mother, my brave father, my amazing brother, my wonderful sister, my titi, my cousin and Nuno that even far away always

supported me and were always there for me. Especially to my parents that have always work so hard and allowed to pursue my dreams. I am so grateful to have you all in my life.

And to you Diogo for being there for me in the good and bad days, for helping me dealing with the stress, for cheering up my days, for being so supportive and give me strength. This experience would not be same without you.

ABSTRACT

Vascular endothelial growth factor (VEGF)-A signal transduction is a central mediator of angiogenesis in development and in pathological conditions, such as ischemic retinopathies. The role of VEGFA in pathophysiological processes including neovascularization and vascular permeability, and the therapeutic benefit of targeting VEGFA and its main receptor on endothelial cells, VEGF receptor-2 (VEGFR2), has been well documented. However, the significant treatment burden for the patient and the transient efficacy of anti-VEGF/VEGFR2 drugs in retinal vascular diseases create a need for new therapeutic targets to improve the diseases´ outcome. Vascular endothelial protein tyrosine phosphatase (VE-PTP, also known as PTPRB) is an endothelial specific tyrosine phosphate that interacts with VEGFR2 and Tie2, thereby regulating their activity. Here, we evaluated the efficiency of a siRNA targeting human *PTPRB* and identified commercially available antibodies specific for VE-PTP to be used in *in vitro* studies. Immunofluorescence analyses of human umbilical vein endothelial cells showed colocalization of VE-PTP with vascular endothelial (VE)-cadherin at endothelial cell junctions, where VE-PTP is known to interact with VEGFR2, Tie2 and VE-cadherin. Silencing of *PTPRB* expression *in vitro* was accompanied by increased VEGFA-induced VEGFR2 phosphorylation at tyrosine site 1175, which unexpectedly was accompanied by decreased phosphorylation of the downstream extracellular regulated kinase (Erk) 1/2. Moreover, endothelial specific genetic deletion of the murine VE-PTP codifying gene, denoted *Ptprb*, impaired retina vascular development, negatively affecting retina vessel density, vessel outgrowth and tip cell density. These effects on the retina vasculature did not depend on changes in expression levels of *Flk1*, *Tie2* or *Cdh5*. In a mouse model of oxygen-induced retinopathy (OIR), genetic *Ptprb* deficiency reduced vessel obliteration but had no effect on formation of neovascular tufts. In conclusion, we demonstrate that VE-PTP is required *in vivo* for normal development of the retinal vasculature and inhibition of *PTPRB* expression *in vitro* markedly enhances VEGFR2 phosphorylation in response to VEGFA while subsequent activation of its downstream signalling transducer Erk 1/2 is suppressed. This suggests a potential mechanism by which targeting VE-PTP may reduce vessel obliteration observed in ischemic eye diseases. However, more in-depth analyses are warranted.

Keywords: VE-PTP, VEGFA, VEGFR2, Erk 1/2, OIR, retinopathy.

RESUMO

A transdução de sinal do *vascular endothelial growth factor* (VEGF)-A é um dos principais mediadores da angiogénese durante o desenvolvimento e em condições patológicas como retinopatias isquémicas. O papel do VEGFA em processos fisiopatológicos, incluindo a neovascularização e a permeabilidade vascular, e o benefício de terapias que têm como alvo o VEGFA e o seu recetor principal nas células endoteliais, o VEGF recetor-2 (VEGFR2), tem sido bem documentados. Contudo, a carga significativa do tratamento para o paciente e a eficácia transitória dos medicamentos anti-VEGF/VEGFR2 em doenças vasculares da retina criam a necessidade de novos alvos terapêuticos para melhorar o resultado do tratamento. A *vascular endothelial protein tyrosine phosphatase* (VE-PTP, também conhecida como PTPRB) é uma fosfatase de tirosinas, especificamente expressa em células endoteliais, que interage com o VEGFR2 e o Tie2, regulando assim a atividade destes. Neste trabalho, avaliámos a eficiência de um siRNA direcionado ao *PTPRB* humano e identificámos anticorpos comerciais específicos para a VEPTP para serem usados em estudos *in vitro*. Análises de imunofluorescência de células endoteliais da veia umbilical humana revelaram que a VE-PTP se localiza com a *vascular endothelial* (VE)-*cadherin* nas junções de células endoteliais, onde se sabe que a VE-PTP interage com o VEGFR2, Tie2 e VE-cadherin. O silenciamento da expressão do *PTPRB in vitro* aumentou a fosforilação do VEGFR2, induzida pelo VEGFA, na tirosina 1175, o qual inesperadamente foi acompanhado por uma diminuição na fosforilação da *extracellular regulated kinase* (Erk) 1/2. Além disso, a deleção genética do gene que codifica a VE-PTP, denominado *Ptprb*, em células endoteliais prejudicou o desenvolvimento vascular na retina afetando negativamente a densidade vascular, o crescimento vascular e a densidade de *tip cells* na retina. Estes efeitos na vasculatura da retina não dependem de mudanças nos níveis de expressão de *Flk1*, *Tie2* ou *Cdh5*. Num modelo de ratinho de retinopatia induzida com oxigénio (OIR), a deficiência genética do *Ptprb* reduziu a obliteração da vasculatura, mas não afetou a formação de *tufts* neovasculares. Concluindo, neste trabalho demonstramos que a VE-PTP é necessária *in vivo* para o normal desenvolvimento da vasculatura da retina e que a inibição da expressão de *PTPRB in vitro* aumenta significativamente a fosforilação do VEGFR2 em resposta ao VEGFA enquanto que a subsequente ativação do seu transdutor de sinalização *downstream* Erk 1/2 é suprimida. Isto sugere um potencial mecanismo pelo qual ter como alvo a VE-PTP pode reduzir a obliteração dos vasos sanguíneos observada em doenças isquémicas dos olhos. Contudo, análises mais aprofundadas são necessárias.

Palavras-chave: VE-PTP, VEGFA, VEGFR2, Erk 1/2, OIR, retinopatia.

CONTENTS

LIST OF FIGURES

ABBREVIATIONS

AJs	Adherens junctions
ANGPT1	Angiopoietin-1
ANGPT2	Angiopoietin-2
bFGF	Basic fibroblast growth factor
bp	Base pair
BSA	Bovine serum albumin
cDNA	Complementary deoxyribonucleic acid
CRISP	Clustered regularly interspaced short palindromic repeat
DAPI	4′,6-diamidino-2-phenylindole
DEP1	Density-enhanced phosphatase 1
DLL4	Delta-like ligand 4
DNA	Deoxyribonucleic acid
Dox	Doxycycline
E	Embryonic day
ECM	Extracellular matrix
ECs	Endothelial Cells
eNOS	Endothelial nitric oxide synthase
EPHB4	Ephrin type-B receptor 4
Erk	Extracellular signal-regulated kinase
ER-LBD	Estrogen receptor ligand binding domain
FBS	Fetal bovine serum
Flk1	Fetal liver kinase 1
Floxed	*loxP* flanked
FOXO1	Forkhead box protein O1
GA	Gestational age
GAPDH	Glyceraldehyde-3-phosphatase dehydrogenase
GEF	Guanine nucleotide exchange factor
GTPase	Small guanosine triphosphate
HIF	Hypoxia-inducible factor
HSP90	Heat shock protein 90
HUVEC	Human umbilical vein endothelial cell
iECKO	Inducible endothelial cell-specific knockout
IP	Intraperitoneal
kDa	kilo Dalton
KDR	Kinase insert domain receptor

loxP	Locus of crossing over (x)
LPS	Lipopolysaccharide
min	minutes
mRNA	Messenger ribonucleic acid
NADPH	Nicotinamide adenine dinucleotide phosphatase
NV	Neovascularization
OIR	Oxygen-induced Retinopathy
ON	Overnight
P	Postnatal day
p	Phospho
PCR	Polymerase chain reaction
PFA	Paraformaldehyde
PKC	Protein kinase C
PLCγ	Phospholipase Cγ
PTPs	Protein tyrosine phosphatases
RNA	Ribonucleic acid
ROI	Region of interest
ROS	Reactive oxygen species
RPL19	Ribosomal protein L19
RPTP	Receptor protein tyrosine phosphatase
RT-qPCR	Real-time quantitative PCR
rtTA	Reverse tetracycline-controlled transactivator
SEM	Standard error of the mean
siRNA	Small interfering RNA
SMCs	Smooth muscle cells
Tet	Tetracycline
TetO	Tetracycline operon
TIME	Telomerase-immortalized human microvascular endothelial
tTA	Tetracycline-controlled transactivator
VE-cadherin	Vascular endothelial cadherin
VEGF	Vascular endothelial growth factor
VEGFR	Vascular endothelial growth factor receptor
VE-PTP	Vascular endothelial protein tyrosine phosphatase
Y	Tyrosine

1. INTRODUCTION

1.1. The Vascular Endothelium

A key component of the vascular system is the monolayer of endothelial cells (ECs) that coats the inner-most aspect of arteries, veins and capillaries. The endothelium forms a barrier between the bloodstream and the surrounding tissues, thereby being in contact with both extravascular cells and blood components. In addition, it functions as an endocrine organ, with arteries delivering oxygen and nutrients to tissues, veins removing the cellular metabolic waste and capillaries exchanging fluids, solutes and condensed matter between tissue compartments. These highly specialized functions are a result of ECs phenotypic, morphological and physiological differences that arise from the heterogeneity of the vascular system. This heterogeneity across the vascular bed allows ECs to perform in a distinct way in various organs and to play a major role in different tasks, such as the regulation of immune responses, inflammation and angiogenesis (Krüger-Genge et al., 2019). This system is also highly conserved across mammalian species.

Signals released from ECs control and maintain the physiological functions of the vasculature. They are also responsible for the recruitment of other blood vessel components, such as connective tissue, smooth muscle cells (SMCs) and pericytes, reinforcing the importance of ECs for growth and development of the blood-vessel wall as well as for regulation of vessel structure and function (Alberts et al., 2002).

1.1.1. Vasculogenesis and Angiogenesis

Blood vessel formation during mammalian embryonic development and in the adult occurs through two main processes (Figure 1.1). The first process is termed vasculogenesis and involves aggregation of ECs precursors, the angioblasts, which subsequently differentiate to endothelial cells, to form a primitive vascular plexus. The second process is a complex remodelling process, termed angiogenesis, which involves growth of newly formed vessels by sprouting from a pre-existing vessel as well as migration and pruning, resulting in the development of a functional vascular system (Coultas et al., 2005; Jain, 2003; Mori et al., 2010).

The *de novo* formation of a network of blood vessels (vasculogenesis) is a crucial process for embryonic development. During this process vascular endothelial growth factor (VEGF)-

A (also denoted VEGF) initiates the expansion, migration and differentiation of ECs to establish a simple capillary network, the primitive capillary plexus that covers the yolk sac (Dong & Yang, 2018; Jain, 2003). VEGF receptor (VEGFR)-2, also known as Flk1 (Fetal liver kinase 1) or KDR (Kinase Insert domain receptor), whose activation is induced by binding of VEGFA, is also crucial for the formation of the vascular plexus (Coultas et al., 2005; Jain, 2003). Embryos lacking VEGFR2 or expressing half the normal level of VEGFA, die embryonically due to defects in the development of blood vessels (Carmeliet et al., 1996; Ferrara et al., 1996; Shalaby et al., 1995). Therefore, establishment of the vascular plexus is a process that requires the activity of VEGFA and VEGFR2-positive angioblasts and is known to be initiated at embryonic day (E)8.5 (Dong & Yang, 2018).

Once the primitive vascular plexus is established, new blood vessels start to gradually form and organize into a functional circulation, in a process known as angiogenesis. ECs remain in a quiescent state in normal physiological conditions. However, during development as well as in the adult, angiogenesis is induced. Thus, during wound healing or in pathological processes such as cancer, quiescent vessels are activated by several growth and transcription factors that control a chain of molecular and cellular events that subsequently leads to formation of a mature vasculature (Alberts et al., 2002; Krüger-Genge et al., 2019).

Sprouting angiogenesis is initiated in response to hypoxia, which increases the intracellular concentrations of the transcription factor hypoxia-inducible factor (HIF)-1 (Alberts et al., 2002; Jain, 2003). In addition, it upregulates the expression levels of different genes, such as *VEGF*, *eNOS* (endothelial nitric oxide synthase) and *ANGPT2* (angiopoietin-2), that act on nearby ECs promoting vessel formation and maturation (Jain, 2003). The EC response entails a sequence of steps: activation of quiescent ECs, sprouting, anastomosis and maturation into a new quiescent status. First, proteolytic degradation of the basement membrane occurs through matrix metalloproteases, allowing interaction between cells and the extracellular matrix (ECM) (Carmeliet & Jain, 2011; Jain, 2003; Krüger-Genge et al., 2019). VEGF selects sensitive ECs, with higher expression of VEGFR2 compared to the neighbouring cells, to become tip cells. The tip cell guides the vessel sprout at the forefront and extends numerous filapodia, able to sense environmental guidance signals for directed migration (Krüger-Genge et al., 2019). Stalk cells are the neighbouring cells of tip cells, less sensitive to VEGF, which are designated to elongate the sprout, proliferate and establish the lumen. This process is also regulated by other signalling mechanisms and proteins that tightly control and restrict the activation of the stalk cells. Briefly, when VEGF binds to VEGFR2 on tip cells, expression of the Notch ligand delta-like ligand 4 (DLL4), is upregulated in a growth factor gradient-dependent manner, controlling the development of new vessel sprouts. DLL4 activates Notch on stalk cells, downregulating VEGFR2 expression, which decreases the responsiveness to VEGFA. Thereby, the stalk cell phenotype is maintained. The sprouting angiogenesis process culminates with the anastomosis of two tip cells of opposing branches, guided by tissue-resident macrophages, allowing blood flow through the new vessel (Carmeliet & Jain, 2011; Fantin et al., 2010; Krüger-Genge et al., 2019). Subsequently, ECs acquire a quiescent phenotype, while pericytes and SMCs stabilize the newly formed vessel (Carmeliet & Jain, 2011; Krüger-Genge et al., 2019).

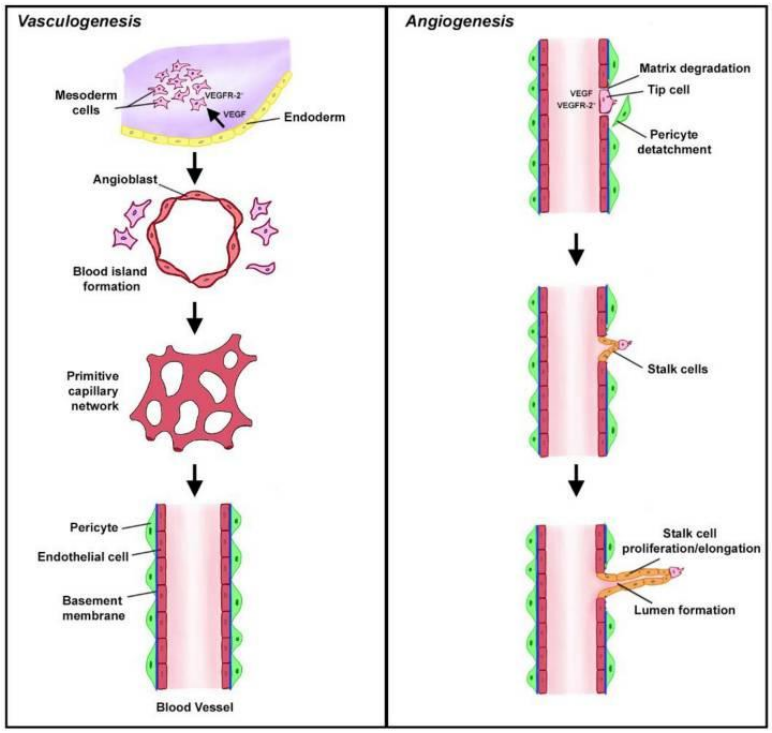

Figure 1.1. Overview of the vasculogenic and angiogenic processes. Vasculogenesis in embryos (left) is the *de novo* creation of new vasculature from primitive mesodermal cells that express VEGFR2. VEGF released from neighbouring endodermal cells converts these VEGFR2+ cells into angioblasts surrounding the blood islands. These islands fuse to form the primitive vascular network that eventually converts into the arteriovenous system. In contrast, angiogenesis (right) is the formation of new vessels from the existing vasculature. The initial steps involve degradation of the extracellular matrix (ECM), detachment of pericytes, and tip formation. The non-proliferating tip endothelial cells move toward proangiogenic factors and are followed by dividing stalk cells (reproduced from Markiewski et al., 2020).

1.2. Vascular Permeability in Health and Disease

Vascular permeability is a process in which ECs establish a dynamic barrier between the blood and the tissue allowing the extravasation of plasma constituents (Claesson-Welsh, 2015; Claesson-Welsh et al., 2021). Under normal physiological conditions, molecules smaller than 40 kDa spontaneously pass through the endothelial barrier, while large molecules need active disruption of the vascular barrier (Claesson-Welsh, 2015). The different functions of ECs in different segments of the microvasculature, result in increased permeability from arterioles (lower) to venules (higher), when leakage is induced (Claesson-Welsh, 2015; Claesson-Welsh et al., 2021). The mechanism that controls vascular leakage and endothelial junctions may differ between different organs. There are two main pathways, transcellular and paracellular, by which active transport across the endothelial occurs. Transcellular permeability requires the formation of transendothelial channels from vesicular vacuolar organelles or fenestrae while paracellular pathway involves transient opening of tight and adherens junctions (AJs) between adjacent ECs (Azzi et al., 2013; Claesson-Welsh, 2015; Radeva & Waschke, 2018). Disruption of AJs occurs in response to several inflammatory mediators, such as VEGFA, histamine and bradykinin (Claesson-Welsh, 2015). The main component of AJs is vascular endothelial (VE)-cadherin, a transmembrane protein exclusively expressed in the en-

dothelium. VE-cadherin is composed of an extracellular region made up of five immunoglobulin-like domain repeats, a single transmembrane domain and a short intercellular region. VE-cadherin extracellular domain mediates the homophilic interaction between cadherins of adjacent cells, while its transmembrane domain participates in lateral clustering within the same cell, such as VEGFR2. Through its cytoplasmic region, VE-cadherin binds to p120-catenin, β-catenin and γ-catenin (plakoglobin), associations that serve a critical role in maintenance of AJs integrity (Azzi et al., 2013; Claesson-Welsh, 2015; Radeva & Waschke, 2018).

Vascular permeability, in physiological settings, is regulated by opening and closing of endothelial junctions, which in part is dependent on VE-cadherin internalization, degradation and recycling (Claesson-Welsh, 2015; Claesson-Welsh et al., 2021). VE-cadherin phosphorylation occurs in response to intermediate levels of flow in venules but not at high shear stress such as in arteries (Orsenigo et al., 2012). In response to permeability modulators, such as inflammatory cytokines and growth factors, levels of tyrosine phosphorylation of VE-cadherin increase further (X. Li et al., 2016). As a consequence, discrete gaps are established at endothelial junctions, leading to increased vascular permeability, in a process triggered by Src family kinases. Activation of other pathways including Rho family guanosine triphosphates (GTPases), which mediate changes in the endothelial cytoskeleton, also contributes to destabilization of the endothelial barrier (Claesson-Welsh, 2015; Claesson-Welsh et al., 2021). Maintenance of AJs through VE-cadherin dephosphorylation can be accomplished by junction-associated protein tyrosine phosphatases (PTPs) including vascular endothelial protein tyrosine phosphatase (VE-PTP) and density-enhanced phosphatase 1 (DEP1) (Azzi et al., 2013; Radeva & Waschke, 2018).

In the quiescent endothelium, endothelial barrier stability is tightly regulated in order to maintain homeostasis. In healthy organs, increased permeability (hyperpermeability) can occur in a reversible way as a result of a transient stimulus, which happens in acute inflammation. Increased permeability, can however be sustained in chronic inflammation, in which the disintegration of the vascular barrier contributes to multi-organ failure. Uncontrolled and exaggerated increase in vascular permeability contributes to diseases such as arthritis, cancer, ischemic stroke, retinopathies, among others, and it can result in edema, inflammation, impaired function and often disease progression (Claesson-Welsh, 2015; Claesson-Welsh et al., 2021; Radeva & Waschke, 2018).

The vasculature in such diseases displays an abnormal phenotype with unstable, leaky vessels and impaired blood flow. It is well established that defects in tumor vessels contribute to a hypoxic microenvironment, which in turn supports uncontrolled angiogenesis through increased expression of pro-angiogenic molecules, such as VEGF. This deterioration of the normal vasculature is accompanied by poor perfusion and increased interstitial pressure, interfering with anti-tumor drug delivery (Azzi et al., 2013; Claesson-Welsh, 2015; Claesson-Welsh et al., 2021). Also in retinal diseases, such as diabetic retinopathy, retinal vein occlusions and age-related macular degeneration, loss of normal vessel function results in ischemia and therefore increased VEGF expression, which leads to excess vascular permeability and disease progression (Claesson-Welsh, 2015). Anti-angiogenic therapies that promote normalization of vessel function and structure by targeting and neutralizing permeability-inducing

modulators, such as VEGF, could improve drug delivery in cancer as well as stabilize and reverse vision loss in eye diseases (Ferrara & Adamis, 2016). Indeed, several VEGF blockers have been approved to treat retinal and cancer diseases. However, many patients exhibit or acquire resistance to VEGF inhibitors. Therefore, new clinical treatments that allow more efficient delivery of conventional therapeutics therapies as well as a better understanding of angiogenetic and permeability mechanisms are needed in order to improve current anti-VEGF drugs (Carmeliet & Jain, 2011; Claesson-Welsh, 2015).

1.3. Protein Tyrosine Phosphatases

Protein tyrosine phosphorylation is regulated by kinases and phosphatases in a dynamic balance, which serves to control physiological functions (Tonks, 2006; Xu & Fisher, 2012). In humans, there is a similar number of tyrosine-targeting phosphatases and kinases, illustrating the important role for these enzymes in the regulation of signalling pathways (Corti & Simons, 2017). Protein phosphatases, which are organized in families that differ in structure and mechanism, show a high degree of complexity, functioning as positive or negative regulators, of specific signalling pathways. Classical phosphotyrosine-specific phosphatases are divided into receptor PTPs (RPTP), localized at the cell membrane, and non-receptor PTPs. RPTPs are composed by an extracellular domain that binds secreted ligands or interacts with ECM components, and an intracellular conserved catalytic domain endowed with phosphatase activity. The catalytic domain is regulated through reactive oxygen species (ROS) mediated oxidation inactivation (Corti & Simons, 2017; Tonks, 2006). The twenty one RPTPs, subdivided into eight sub-families, display different extracellular domain compositions (Tonks, 2006; Xu & Fisher, 2012).

Disruption of PTP function is associated with several human diseases, such as cancer, diabetes and hereditary disorders. Unfortunately, development of drugs that target the active site of PTPs is challenging due to its highly conserved cysteine residue that makes it difficult to selectively inhibit the activity of a specific PTP. Also the active site is positively charged, preferentially binding negatively charged molecules, which usually lack cell permeability. However, development of appropriate nonhydrolyzable molecules that mimic the ligand binding to the active site and that bind less conservative secondary-substrates sites flanking the active site, have shown to be highly potent and selectively inhibit PTP activity in *in vivo* animal models of oncology, diabetes/obesity, autoimmunity, and tuberculosis (Zhang, 2017). Understanding the signalling and mechanisms underlying RPTPs physiological functions is a prerequisite for development of new potent, selective and bio-active inhibitors, which may provide new approaches to treat human disease (Corti & Simons, 2017; Tonks, 2006; Xu & Fisher, 2012; Zhang, 2017).

1.4. Vascular Endothelial Protein Tyrosine Phosphatase

VE-PTP (also denoted PTPRB in human) belongs to the R3 subfamily of RPTPs, characterized by an extracellular domain composed exclusively of fibronectin type III-like domains, and an intracellular catalytic domain (Fachinger et al., 1999; Vestweber, 2021). In contrast to

other tyrosine phosphatase, VE-PTP is specifically expressed on ECs, with a pronounced expression on arterial endothelium of blood endothelial cells (Bäumer et al., 2006). However, VE-PTP is not expressed in lymphatic endothelial cells (Souma et al., 2018; Vestweber, 2021). VE-PTP is highly expressed in the vasculature of most if not all organs in the mouse such as lungs, brain, spleen, kidney and heart as well as in tumor vasculature (Dominguez et al., 2007; Fachinger et al., 1999).

Endothelial selectivity of VE-PTP to ECs is related to its role in controlling endothelial functions. During embryonic development, mice carrying a VE-PTP gene inactivation or that express a truncated form of the protein, die at embryonic day (E)10 as result of severe vascular malformations. Phenotypic alterations in VE-PTP mutant mice comprise growth delay during development and defects in the heart. Moreover, although during vasculogenesis the vascular plexus of the yolk sac can be formed in the absence of VE-PTP expression, it is unable to remodel into hierarchically branched structures, establishing VE-PTP activity as essential for vessel remodelling and angiogenesis (Bäumer et al., 2006; Dominguez et al., 2007). In addition, VE-PTP expression is upregulated during embryonic development when angiogenesis is induced, compared to its expression during vasculogenesis (Dominguez et al., 2007). In adults, VE-PTP functions as an important regulator of vascular permeability, by stabilizing VE-cadherin junctions (Nawroth et al., 2002; Nottebaum et al., 2008). The junction stabilization effect is dependent on VE-PTP´s association with the endothelial specific adhesion molecule VE-cadherin and also with the tyrosine kinase receptors Tie2 and VEGFR2 (Fachinger et al., 1999; Mellberg et al., 2009; Nawroth et al., 2002). Most recently, FGD5 and ephrin type-B receptor 4 (EPHB4) were also identified as direct substrates of VEPTP (Braun et al., 2019; Drexler et al., 2019).

1.4.1. Regulation of VEGFR2 signalling by VE-PTP

In mammals, VEGFR2 is preferentially expressed in ECs and in embryonic precursor cells, but is also found in neuronal cells and hematopoietic stem cells (Corti & Simons, 2017; Wang et al., 2020). VEGFR2 activation is induced by binding of VEGF-A, VEGF-C and VEGF-D, leading to homo- and hetero-dimerization of the receptor followed by conformational changes and autophosphorylation of the tyrosine kinases (Wang et al., 2020). Subsequently, VEGFR2 activation by VEGF induces several downstream pathways, which regulate biological processes such as migration, proliferation and survival as well as enhanced vascular permeability and neovascularization. Interaction of VEGFR2 with its major ligand VEGF-A (also known as vascular permeability factor for its ability to induce vascular leakage), plays an important role in regulation of angiogenesis (Abhinand et al., 2016; Corti & Simons, 2017; Wang et al., 2020). Furthermore, activation of the receptor by VEGF-A can result in phosphorylation of specific intracellular tyrosine (Y) residues, such as Y1175 (Y1173 in mouse), Y951 (949), Y1214 (Y1212), Y1054/1059 (Y1052/1057) (Abhinand et al., 2016; Corti & Simons, 2017; Matsumoto et al., 2005). Phosphorylation of each tyrosine site is linked to activation of specific downstream signalling pathways that control different physiological responses (Olsson et al., 2006).

VE-PTP was found close to the nucleus within endocytic vesicles, but on matured vasculature it is translocated to ECs contacts, where it preferentially localizes and controls barrier function by regulating the activity of its substrates (Hayashi et al., 2013; Nottebaum et al., 2008). In the quiescent endothelium, VE-PTP forms a complex with VEGFR2, as revealed by proximity ligation assay. However, VEGFR2 activation by VEGF induces transient loss of this association, accompanied by a transient increase in VEGFR2 phosphorylation at Y1175. In addition, VE-PTP silencing in immortalized ECs increases VEGF-induced VEGFR2 phosphorylation at Y1175 and Y951, but not at Y1214, while baseline phosphorylation of VEGFR2 is unaffected (Hayashi et al., 2013; Mellberg et al., 2009). The presence of VE-PTP in ECs leads to interaction and dephosphorylation of VEGFR2 tyrosine residues, in a process that requires the presence of Tie2, but not its kinase activity. In the same study, VEGFR2 was found to exist both in complex with Tie2 or in a trimeric complex with Tie2 and VE-PTP (Hayashi et al., 2013). In unstimulated cells, silencing of VE-PTP increases phospho (p)- extracellular signal-regulated kinase (Erk) and p-Akt (also known as protein kinase B) levels, while VEGF stimulation results in a further slight increase in p-Akt (Mellberg et al., 2009). VEGFR2 increased tyrosine phosphorylation and activation of downstream signalling pathways as result of VE-PTP silencing can affect the VEGF-response during angiogenesis and development. Indeed, VE-PTP was shown to be important during endothelial morphogenesis, since abrogation of VE-PTP overcomes cell cycle arrest at G_0/G_1 therefore affecting tubular morphogenesis of 3D cultures (Mellberg et al., 2009). In stalk cells of the sprout, VE-PTP regulates VEGFR2 activity and its ablation results in immature sprouts due to excess VEGFR2 activity accompanied by reduced perycite coating. Furthermore, VE-PTP silencing and subsequent increase in p-VEGFR2, increases VE-cadherin phosphorylation (Figure 1.2), which in mouse embryoid bodies, tumors and inter-somitic vessels in developing zebrafish results in loss of cell polarity and lumen formation, supporting VE-PTP´s crucial role in these processes (Hayashi et al., 2013).

1.4.2. Other VE-PTP substrates

1.4.2.1. VE-cadherin

VE-cadherin is a component of endothelial junctions essential for the maintenance of vascular integrity and the formation of blood vessels (Giannotta et al., 2013). Gene inactivation of VE-cadherin leads to embryonic lethality at E9.5, due to defects in vessel maturation and remodelling (Carmeliet et al., 1999). In addition, VE-cadherin is necessary for correct vascular connections and inhibition of sprouting activity, supporting its important role during vascular development. Partial reduction of VE-cadherin expression is sufficient to prevent formation of a stable vasculature, therefore partial inhibition of internalization or a change in function of VE-cadherin may strongly affect vascular stability and organization (Montero-Balaguer et al., 2009). Moreover, VE-cadherin tyrosine phosphorylation at Y685 induces vascular permeability, while dephosphorylation at Y731 via the tyrosine phosphatase Src homology phosphatase-2 leads to leukocyte extravasation. In both processes VE-cadherin endocytosis is induced, supporting the important role for VE-cadherin in the control of endothelial junction integrity and vascular permeability (Arif et al., 2021; Orsenigo et al., 2012; Wessel et al., 2014).

VE-PTP was shown to associate with VE-cadherin *in cis* through the membrane-proximal extracellular domain of each protein. In the same study, VE-PTP was able to reduce VEGFR2-induced VE-cadherin phosphorylation and cell layer permeability independently of its enzymatic activity (Nawroth et al., 2002). Further studies, showed that VE-PTP regulates vascular permeability by controlling VE-cadherin phosphorylation at Y685 (Wessel et al., 2014). In contrast, silencing of VE-PTP increased phosphorylation at Y685 as well as ECs permeability and leukocyte extravasation, in a process that required dissociation of VE-PTP from VE-cadherin (Broermann et al., 2011; Wessel et al., 2014). Dissociation of the two molecules was shown to happen *in vitro* in response to leukocyte binding to tumor necrosis factor α activated ECs as well as *in vivo* upon lipopolysaccharide (LPS)-induced leukocyte extravasation, and also both *in vivo* and *in vitro* in response to VEGF (Broermann et al., 2011; Nottebaum et al., 2008). The signalling mechanism behind this process is triggered by several different mechanisms; binding of leukocytes to the vascular cell adhesion molecule 1, stimulation with VEGF that activates the small GTPase Rac1, the generation of ROS via nicotinamide adenine dinucleotide phosphatase (NADPH) oxidase and the activation of the tyrosine kinase Pyk2 (Figure 1.2) (Vockel & Vestweber, 2013). Disruption of endothelial junctions is accompanied by increased VE-cadherin, β-catenin and plakoglobin tyrosine phosphorylation. However, only plakoglobin is necessary for VE-PTP´s support of the adhesive function of VE-cadherin. Moreover, plakoglobin was identified as a substrate for VE-PTP using a trapping mutant of VE-PTP (Nottebaum et al., 2008). Stimulation of ECs with thrombin, a permeability-increasing mediator, leads to stromal interaction molecule 1 activated Ca^{2+} entry and subsequent activation of Pyk2, which mediates VE-PTP phosphorylation at Y1981 facilitating binding and activation of Src and subsequent VE-cadherin phosphorylation linked to disruption of endothelial junctions (Soni et al., 2017).

Regulation of VE-cadherin function by VE-PTP was also shown in tumors. In metastatic melanoma cells, VE-PTP can form a complex with VE-cadherin and p120-catenin, preventing VE-cadherin degradation, which leads to the formation of perfusion pathways in the tumor, by a process known as vascular mimicry. In contrast, silencing of VE-PTP enhances VE-cadherin autophagy and disruption of vascular mimicry formation (Delgado-Bellido et al., 2020). In the quiescent endothelium, VE-PTP reduces VE-cadherin internalization rate, thereby restricting endothelial permeability by stabilizing VE-cadherin junctions in a manner that is independent of VE-PTP phosphatase activity. In this process, VE-PTP serves as an adaptor protein that directly interacts with the Rho family guanine nucleotide exchange factor (GEF)-H1 (also known as ARHGEF2) inhibiting its binding to RhoA, thereby reducing RhoA activity and tension across VE-cadherin junctions (Juettner et al., 2019). VE-cadherin internalization was also restricted in hypoxic conditions due to increased expression of the transcription factor HIF2α accompanied by enhanced VE-PTP expression, which prevented loss of endothelial barrier function (Gong et al., 2015). Therefore, VE-PTP´s supportive role of VE-cadherin function is important for maintenance of junctional integrity and regulation of vascular permeability.

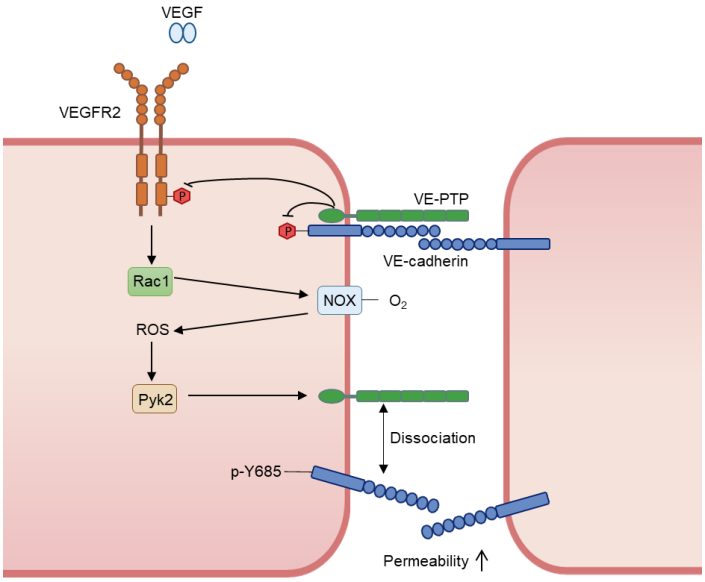

Figure 1.2. Role of the VE-PTP substrates VE-cadherin and VEGFR2 for endothelium barrier function. VE-PTP associates with and supports the function of VE-cadherin by blocking its phosphorylation as well as the phosphorylation of VEGFR2, thereby counteracting VEGF-induced dissociation of VE-cadherin complexes between adjacent endothelial cells. VEGF (and also other pro-inflammatory factors) induces the dissociation of VE-PTP from VE-cadherin via a mechanism based on the activation of Rac1, the generation of ROS via NADPH oxidase, and the activation of the kinase Pyk2. This dissociation is necessary to inhibit the function of VE-cadherin.

1.4.2.2. **Tie2**

Tie2 is a receptor tyrosine kinase that belongs to the angiopoietin/Tie signalling family, being the principal mediator of the vascular functions attributed to this pathway. Activity of the receptor Tie2 is controlled by its ligands angiopoietin 1-4. The ligands Angiopoetin-1 (ANGPT-1) and ANGPT2 are the best characterized members of this family (Akwii & Mikelis, 2021; Bilimoria & Singh, 2019; Eklund & Olsen, 2006). ANGPT1 is produced by non-ECs and induces its activity on ECs by acting directly on the endothelium or by recruiting mural cells, while ANGPT2 is expressed by ECs, stored in the cytoplasm of these cells in Weibel-Palade bodies and can be released under hypoxic and inflammatory conditions. ANGPT1 acts mainly as an agonist and binding of the ligand to Tie2 induces receptor autophosphorylation, thereby initiating a cascade of downstream signals that promote vascular stability (Akwii & Mikelis, 2021; Eklund & Olsen, 2006). These signals can activate different signalling pathways that trigger distinct vascular functions, such as survival, migration, sprouting and cytoskeletal remodelling (Bilimoria & Singh, 2019; Eklund & Olsen, 2006). In addition, ANGPT1 has an anti-inflammatory role during inflammation and an anti-permeability role, counterbalancing the increasing permeability effect of VEGF (Akwii & Mikelis, 2021; Bilimoria & Singh, 2019). In contrast, ANGPT2 is a context-dependent antagonist or agonist, depending on the tissues environment (Eklund & Olsen, 2006). As an antagonist, ANGPT2 mainly blocks ANGPT1-induced Tie2 phosphorylation, inhibiting vascular quiescence and stability. ANGPT2 acts as an agonist in the absence of ANGPT1 and during lymphatic development (Akwii & Mikelis, 2021; Bilimoria & Singh, 2019; Eklund & Olsen, 2006). Moreover, Tie1 presence can determine the context-dependent role of ANGPT2 (Akwii & Mikelis, 2021). Under physiologic conditions, Tie1 interacts with Tie2 supporting ANGPT2 agonist function. However, in inflammation Tie1 cleavage triggers ANGPT2 antagonist activity leading to loss of vascular stability

(Korhonen et al., 2016). Mechanistically, the antagonistic effect of ANGPT2 on Tie2 involves a feedback loop, in which activation of forkhead box protein O1 (FOXO1) increases ANGPT2 expression leading to vascular remodelling and leakage (M. Kim et al., 2016).

The binding of ANGPT1 to Tie2, a vascular-specific receptor tyrosine kinase, has an established role in vascular function, regulating angiogenesis, cell survival, vascular permeability, and inflammatory responses (Akwii & Mikelis, 2021; Bilimoria & Singh, 2019). Tie2 and ANGPT1 deficient mice show similar vascular phenotypes and die embryonically around E9.5 and E12.5, respectively, due to lack of remodelling of the primary plexus (Akwii & Mikelis, 2021; Eklund & Olsen, 2006). These data supports the critical role of ANGPT1/Tie2 during development, in blood vessel remodelling and maturation. In the adult, Tie2 is mainly required for maintenance of a mature, quiescent phenotype of the vasculature (Eklund & Olsen, 2006).

Another important component of the angiopoietin/Tie2 pathway is VE-PTP, whose function involves binding through its cytoplasmic domain to Tie2 and in this manner it regulates Tie2 activity by reducing its tyrosine phosphorylation (Figure 1.3) (Fachinger et al., 1999; Goel et al., 2013). In addition to Tie1, VE-PTP was shown to steer the context-dependent function of ANGPT2. The absence of VE-PTP expression in the lymphatic vasculature allows ANGPT2 to exert its agonistic function, permitting ANGPT2/Tie2-mediated lymphangiogenesis (Souma et al., 2018). Dissociation of VE-PTP from Tie2 increases tyrosine phosphorylation of Tie2, resulting in activation of its downstream signalling target Erk 1/2 that leads to enhanced EC proliferation and enlargement of vascular structures (Winderlich et al., 2009). Gene disruption of VE-PTP is also associated with enlargement of the blood vessels and defects in vascular remodelling (Bäumer et al., 2006). Thus, VE-PTP is required to balance Tie2 activity, thereby controlling ECs proliferation and vascular remodelling during embryonic development (Winderlich et al., 2009). In mouse teratomas, VE-PTP-mediated control of Tie2 activity was also confirmed to regulate the size of tumor vessels (Z. Li et al., 2009). Inhibition of VE-PTP by gene ablation, with antibodies and AKB-9778 (razuprotafib), a pharmacological inhibitor of VE-PTP, prevents LPS-, VEGF-, histamine- and ANGPT2 induced permeability and leukocyte extravasation in mice (Frye et al., 2015; Gurnik et al., 2016). These effects required expression of Tie2, since blocking VE-PTP in the absence of Tie2 lead to destabilization of endothelial junctions, which is in line with VE-PTP´s support of VE-cadherin function. Mechanistically, inhibition of VE-PTP stabilizes endothelial junctions via ANGPT1 binding to Tie2, subsequent translocation to EC contacts and activation of the receptor, which triggers activation of Rap1 leading to Rac1 activation, thereby reducing radial stress fiber formation and nonmuscle myosin II (Figure 1.4). Moreover, VE-PTP´s stabilizing effect on endothelial junctions via Tie2 occurs by a mechanism independent of VE-cadherin. Therefore, inflammatory-induced weakening of endothelial junctions requires not only targeting of VE-cadherin and/or associated proteins but also interference with the actomyosin system. The latter effect is dampened by Tie2 activation (Frye et al., 2015).

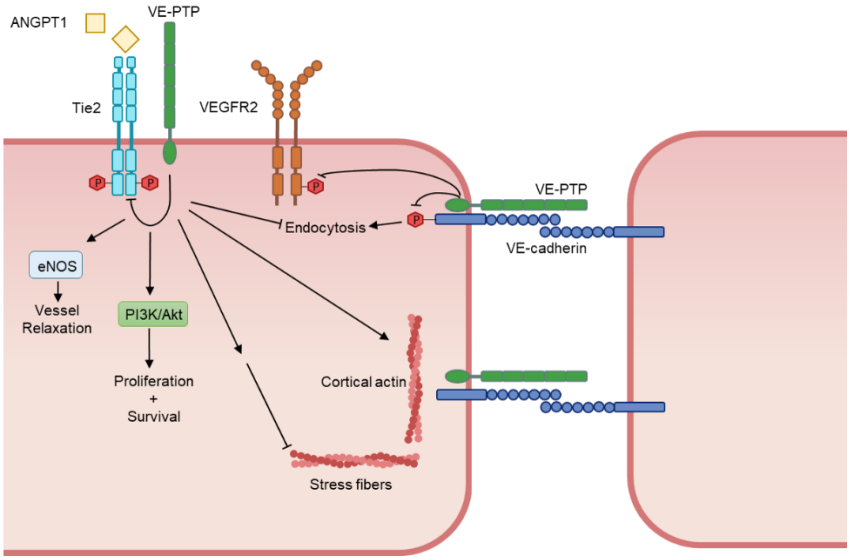

Figure 1.3. Role of the VE-PTP substrate Tie2 for endothelium barrier function. Inhibition of VE-PTP triggers the activation of Tie-2, which supports survival and proliferation, leads to vessel relaxation by activating eNOS, and stabilizes endothelial junction integrity by enhancing cortical actin and dampening the activity of actin stress fibers (explained in more detail in FGD5 section). Although VE-PTP inhibition acts negatively on VE-cadherin and leads to the phosphorylation of VE-cadherin and associated catenins, VE-cadherin endocytosis is counteracted by Tie-2 activation. Furthermore, reduced VE-cadherin adhesive activity may be compensated by a Tie-2-induced lack of actomyosin-based pulling forces on junctions.

1.4.2.3. **FGD5**

The FGD (FYVE, RhoGEF, and PH domain containing) 5 is a Cdc42 GEF, specifically expressed in hematopoietic stem cells and in ECs. It belongs to the FGD GEF family that consists of FGD 1 to 6. The various FGD protein interactions allow membrane remodelling and receptor trafficking. FGD5 plays a role in regulating cytoskeletal remodelling, in a process that occurs after VEGF activation of VEGFR2. It also controls VEGFR2 trafficking and assembly with mTOR complex-2 and Akt on the early endosome. In addition, FGD5 modulates phosphatidylinositol 3-kinase signalling, regulating in this manner endothelial adhesion, survival and angiogenesis. Therefore, it is essential during embryonic development and in vascular patterning. Expression of FGD5 is also found in highly vascularized organs, such as the kidney, and it is upregulated upon VEGF stimulation (Eitzen et al., 2018). In ECs, overexpression of FGD5 leads to disordered retinal vascular development in the mouse postnatal retina, which supports that in normal conditions expression of FGD5 must be tightly controlled (Cheng et al., 2012).

FGD5 was found to be a direct substrate of VE-PTP (Braun et al., 2019). Inhibition of VE-PTP was previously described to stabilize endothelial junctions and counteract inflammation-induced destabilization via activation of the ANGPT1/Tie2 signalling pathway. In addition, VE-PTP ablation and subsequent activation of the Tie2 pathway overrides the junction destabilization effect (Frye et al., 2015). In contrast, the junction-stabilizing effect of VE-PTP through ANGPT1/Tie2 signalling is inhibited under histamine and thrombin stimulation, upon FGD5 ablation. Moreover, VE-PTP inhibition leads to increased phosphorylation of FGD5 at Y820, which prevents barrier-disruption. This is a two-step process in which Tie2 activation upon VE-PTP inhibition induces first the translocation of FGD5 to endothelial junctions by activa-

tion of Rap1 and secondly, FGD5 becomes phosphorylation at Y820 by Tie2 (directly or indirectly), resulting in full activation and function of FGD5 (Figure 1.4). Activation of FGD5 leads to activation of Cdc42 and Rac1, required for the formation of cortical actin bundles at cell contacts and inhibition of radial stress fiber formation (Braun et al., 2019). Therefore, FGD5 is important in Tie2-stimulated phosphorylation control of vascular leakage. Moreover, FGD5 is essential *in vivo* for prevention of plasma leakage during leukocyte extravasation. In this process, ANGPT1 is released from platelets, leading to activation of Tie2 and in turn phosphorylation of FGD5. Activation of FGD5 induces reinforcement of cortical actin bundles and constricts the diapedesis pore during the transmigration process, preventing plasma leaks (Braun et al., 2020; Vestweber, 2021).

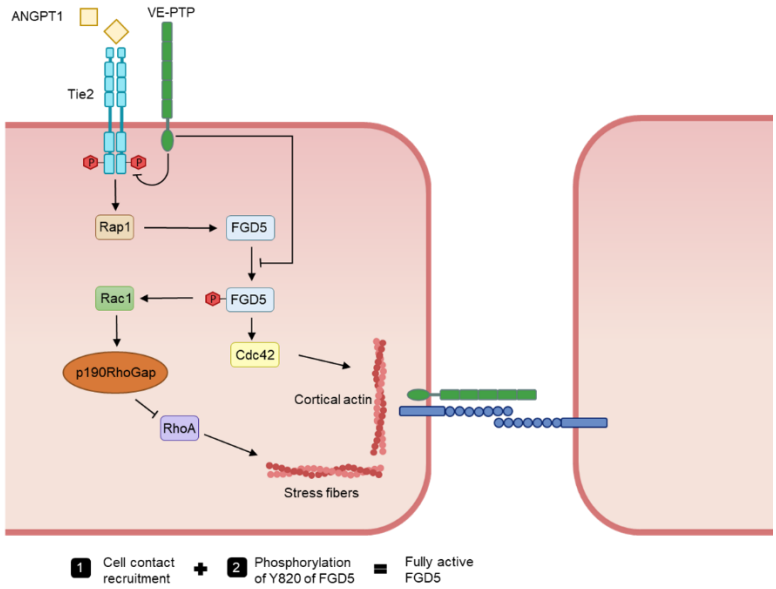

Figure 1.4. Role of the VE-PTP substrate FGD5 for endothelial barrier function. Inhibition of VE-PTP stabilizes endothelial junction integrity by activating Rap1, which targets indirectly the activation of Rac1 that in turn dampens Rho activity via p190RhoGAP, thereby dampening pulling forces on junctions by radial stress fibers. The putative exchange factor FGD5 is a key component in this cascade. It is a direct substrate for VE-PTP as well as a downstream target for Tie-2 kinase. FGD5 becomes recruited to junctions via Rap1 activation. In addition, FGD5 becomes fully activated by phosphorylation at Y820, which is needed for activation of Cdc42 and strengthening of cortical actin and for activation of Rac1 and inhibition of stress fibers formation.

1.4.2.4. **EPHB4**

The tyrosine kinase EPHB4 has an important physiological role during vascular development and postnatal angiogenesis (Du et al., 2020). Deletion of EPHB4 in mice leads to embryonic lethality due to various cardiovascular defects (Gerety et al., 1999). EPHB4 is predominantly expressed on venous ECs and its expression is upregulated in tumor cells (Du et al., 2020; Gerety et al., 1999). Activity of the EPHB4 receptor is regulated by binding of its major ligand EphrinB2, which is essential for vascular remodelling of primitive capillary networks into distinct arteries and veins. During angiogenesis, VEGF upregulates EphrinB2 expression, which is accompanied by EPHB4 down-regulation (Du et al., 2020). In addition, EphrinB2/EPHB4 signalling promotes sprouting and maturation of new blood vessels. In adult angiogenesis, EPHB4 participates in pathophysiological processes, such as wound healing, the female reproductive cycle, tumorigenesis, ischemic cardiovascular disease and ocular

angiogenesis (Du et al., 2020; Yang et al., 2016). Moreover, some EPH receptors have been recognized as substrates of R3 family of PTPs (Sakuraba et al., 2013).

EPHB4 was most recently identified as a substrate of VE-PTP. As a result, increased tyrosine phosphorylation of EPHB4 was observed upon VE-PTP inhibition. EPHB4 forms a ternary complex together with VE-PTP and Tie2, but EPHB4 and Tie2 trigger independently distinct signalling pathways and trans-activation of the receptors is not observed even in the absence of VE-PTP (Drexler et al., 2019). These findings suggest a role for VE-PTP in balancing the activity of both receptors and their corresponding signalling pathway. Furthermore, the formation of the VE-PTP, EPHB4 and Tie2 ternary complex could explain the decrease in tumor vascular permeability via EPHB4 activation of ANGPT1/Tie2 signalling pathway (Erber et al., 2006).

1.4.3. Potential Therapeutic Effects of Targeting VE-PTP

The VEGF/VEGFR2 pathway has been the most common target of ophthalmological therapies. However, the benefit of VEGF therapies is limited by the requirement for periodic and repetitive administration (Akwii & Mikelis, 2021). The angiopoietin/Tie2 pathway plays an essential function in maintaining vascular integrity. Thus, regulators of this pathway are potential targets for the treatment of pathological conditions characterized by pathological angiogenesis and excessive vascular permeability.

In some diseases accompanied by development of hypoxia and low oxygen tension, such as in diabetes and ischemic retinopathy, VE-PTP expression becomes upregulated *in vivo*, thereby reducing Tie2 activity (Carota et al., 2019; Shen et al., 2014). VE-PTP´s negative regulatory effect on ANGPT/Tie pathway, makes it a potential therapeutic target. Indeed, a pharmacological inhibitor of VE-PTP was developed, AKB-9778 (razuprotafib) (Aerpio Pharmaceuticals). AKB-9778 binds to VE-PTP´s catalytic domain inhibiting its phosphatase activity, thereby leading to stabilization of endothelial junctions (Akwii & Mikelis, 2021). In murine mammary carcinoma, AKB-9778 was shown to normalize the tumor vasculature by activating Tie2 signalling independently of the ligand context. This resulted in early phase tumor growth delay, slower progression of micrometastases and enhanced response to concomitant cytotoxic treatments. VE-PTP inhibition also increased eNOS phosphorylation at the serine 1177 residue, which normalized tumor vessel structure and function, improved perfusion and reduced hypoxia, which in turn is linked to better prognosis (Goel et al., 2013). Similar effects were observed upon VE-PTP inhibition in an *in vivo* mouse model of diabetic kidney disease, in which Tie2 activation is strongly reduced due to high levels of VE-PTP expression in the renal vasculature. VE-PTP gene inactivation restored Tie2 activity and increased eNOS phosphorylation, which was accompanied by nuclear exclusion of the transcription factor FOXO1. As consequence, expression of factors that promoted inflammatory responses and fibrosis was reduced, preserving in this manner the kidney structure and function (Carota et al., 2019). Moreover, AKB-9778 was suggested to be a promising therapy for the treatment of ischemic retinopathies. Mice with these diseases have high expression levels of ANGPT2, which stimulates retinal neovascularization (NV). However, treatment with subcutaneous and intraocular injection of AKB-9778 induces Tie2 activation and strongly suppresses NV in a mouse

model of neovascular age-related macular degeneration. In addition, AKB-9778 also prevented exudative retinal detachment, suggesting it to be a promising therapy for retinal and choroidal vascular diseases (Shen et al., 2014).

In clinical trials, AKB-9778 was tested as a novel treatment in ocular normotensive patients with diabetic eye diseases. In phase IIa clinical trials, self-administration of subcutaneous injection of AKB-9778 was shown to decrease intraocular pressure in patients with diabetic macular edema. In accordance, topical ocular administration of AKB-9778 in mice increased Tie2 activity in the endothelium of Schlemm´s canal, facilitating drainage and therefore reducing the intra ocular pressure (G. Li et al., 2020). Moreover, deletion of a single VE-PTP allele rescued the developmental defects observed in Tie2 haploinsufficient mice by increasing Tie2 activity and promoting normal development of Schlemm´s canal (Thomson et al., 2019). Treatment combination of AKB-9778 with ranibizumab, an anti-VEGF monoclonal antibody, enhanced the reduction in diabetic macular edema compared to suppression of VEGF alone (Campochiaro et al., 2016). In phase IIb clinical trials, patients with non-proliferative diabetic retinopathy treated with AKB-9778 once or twice a day for 48 weeks also showed a significant reduction in intraocular pressure compared to the placebo (G. Li et al., 2020). However, phase II clinical trials studies were completed in March 2019 and failed to meet its primary endpoint. Future research on the application of VE-PTP inhibitors as well as combination therapy with anti-VEGF drugs might improve clinical outcome in other diseases such as pulmonary artery hypertension (Akwii & Mikelis, 2021; Drexler et al., 2019).

1.5. In vivo angiogenesis model - Oxygen-induced Retinopathy

The retinal vasculature is one of the most well-known vascular beds in the body. The high metabolic demand of the adult retina is facilitated by two main vascular networks: the retinal vasculature organized in three layers of vessels that supply the inner retina, and the choroidal vasculature that supplies the outer retina pigment epithelium and photoreceptors. During initial development stages, the retina in both human and mouse is supported by a transient vascular network, the hyaloid vessels. These vessels originate from a central artery that enters the optic fissure and progresses to the vitreous surrounding the lens (Akwii & Mikelis, 2021; Dai et al., 2021). At the final stage of retinal development, the hyaloid vessels start to regress and the retina is supported by the retinal vasculature. In humans, hyaloid vessels originate at 6 weeks of gestation age (GA) and regresses at about 13 weeks of GA, while at 16 weeks of GA the retinal vasculature begins to develop. The vasculature starts to form at the optic nerve and extends until it has reached the peripheral edge of the retina, originating the superficial retinal vascular plexus at 36 weeks of GA. Subsequently, the vasculature penetrates into the retina forming the intermediate and deep vascular plexus. Human retinal vascular development occurs in utero and it is fully mature before birth, normally at 40 weeks of GA. In contrast, in mice, the hyaloid vasculature develops embryonically, while the retinal vasculature develops postnatally, by a similar process. In mice, development of the retinal vasculature begins at the postnatal day (P)1, equivalent to 25 weeks of GA in humans,

with retinal arteries extending from the optical nerve towards the peripheral retina. At P8, the superficial retinal vasculature has formed. The formation of the remaining two layers of vessels, occurs between P7 to P12 (Dai et al., 2021). Mice develop a fully mature retinal vasculature at 3 weeks after birth (Scott & Fruttiger, 2009).

Angiogenesis is an important process during vascular development, but also in pathological NV that can be induced by an imbalance between pro- and anti-angiogenic factors (Vähätupa et al., 2020). Oxygen-induced retinopathy (OIR) is an angiogenesis model used to represent ischemic retinopathies, such as retinal vein occlusion, proliferative diabetic retinopathy and retinopathy of prematurity (Scott & Fruttiger, 2009; Smith et al., 1994; Vähätupa et al., 2020). In these diseases, ocular angiogenesis is abnormal, resulting in neovascularization (abnormal vessels). Vascular leakage can occur, which may contribute to vision loss (Scott & Fruttiger, 2009; Vähätupa et al., 2020). The OIR model in mice is an inexpensive model that allows reproducible and quantifiable retinal NV (Smith et al., 1994).

The OIR model consists of two phases (Figure 1.5). In the first phase, P7 mouse pups and their nursing mother are exposed to 75% oxygen until P12 (Dai et al., 2021; Scott & Fruttiger, 2009; Smith et al., 1994; Vähätupa et al., 2020). During this phase, the immature retinal vasculature is exposed to hyperoxia, which supresses the expression of angiogenic factors, such as VEGF, essential for physiological angiogenesis and EC survival in the immature vessels. Hyperoxia interferes with the development of the vasculature causing rapid obliteration of the capillaries in the centre of the retina, where oxygen concentrations are higher. Thereby, a functional network of vessels remains only in the periphery, supplied by radial arteries and venules (Dai et al., 2021; Scott & Fruttiger, 2009). The second phase is initiated when mouse pups and their nursing mother are removed from hyperoxia and returned to normal room air (Dai et al., 2021; Scott & Fruttiger, 2009; Smith et al., 1994; Vähätupa et al., 2020). Upon return to normoxic conditions, the retina experiences a relative hypoxia, which stabilizes HIF-1. Subsequently, it upregulates the expression of angiogenic factors that promote survival, including VEGF. The increase in VEGF levels triggers pathological retinal NV and intravitreal NV at P14 (Dai et al., 2021; Scott & Fruttiger, 2009). In addition, hypoxia leads to vessel sprouting in veins and in the remaining capillaries in the periphery. Some of these retinal blood vessel sprouts fail to regenerate the capillary network and instead form neovascular tufts growing towards the vitreous. These tufts, are hyperpermeable and immature (Dai et al., 2021; Scott & Fruttiger, 2009; Vähätupa et al., 2020). Pathological retinal NV is established from the periphery towards the centre and has its peak at P17. This process is followed by regression of the vasculature with almost complete replacement of abnormal vessels and reestablishment of a normal vasculature at P25 (Connor et al., 2009).

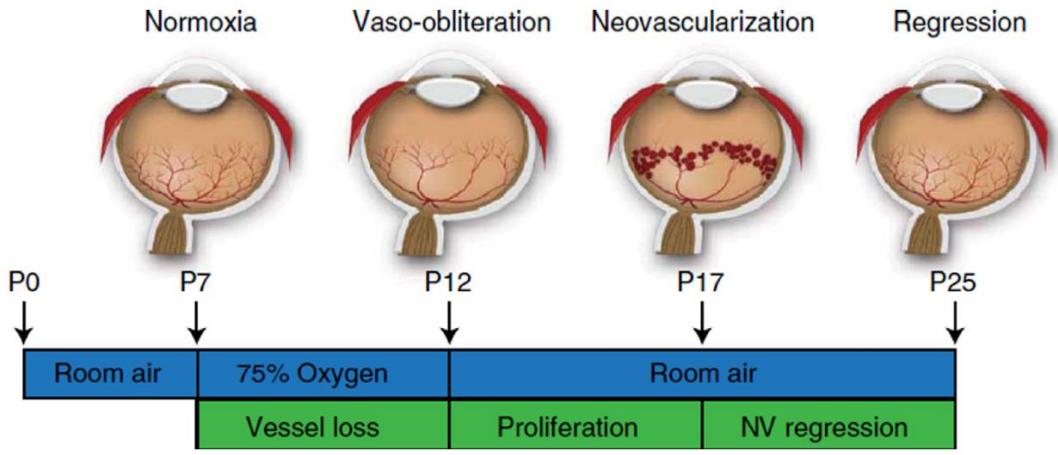

Figure 1.5. Cartoon schematic of the mouse OIR model. Neonatal mice and their nursing mother are kept in room air from birth through P7 and normal vascular development ensues. At P7, mice are exposed to 75% oxygen, which inhibits retinal vessel growth and causes significant vessel loss. Mice are returned to room air at P12; the avascular retina becomes hypoxic, triggering both normal vessel regrowth and a pathological neovascular response. NV reaches its maximum at P17. Shortly thereafter, the NV spontaneously regresses, and the retina reaches resolution by P25 (reproduced from Connor et al., 2009).

Despite the advantages of the OIR model, there are several factors that can lead to phenotypic variabilities that need to be considered. Different mouse strains show variable ocular angiogenesis after OIR in the context of light exposure and expression of angiogenic factors. Therefore, OIR experiments should be conducted in the same strain background obtained from a single vendor. Exposure of nursing mothers to hyperoxia can result in infertility, decrease in lactation and cannibalization. The weight of pups should be measured at P7 and P17 since weight loss is a strong predictor of severity of retinopathy of prematurity. Another limitation of this model is the NV quantification that requires manual counting, grading or tracing of NV, being a time-consuming and somewhat subjective method (C. B. Kim et al., 2016; Stahl et al., 2010). Although, the OIR model mimics and offers a reproducible NV model for retinopathy of prematurity, there are other models that replicate pathological angiogenesis in the mouse retina. An example of this is laser-induced choroidal NV, which is a preferable model to study the wet form of age-related macular edema. However, lack of perfect animal models that recapitulate some human ischemic eye diseases, such as diabetic retinopathy, remains an unmet need (Stahl et al., 2010).

Angiopoietin/Tie2 and VEGF/VEGFR2 pathways are essential in retinal vascular development and maintenance. However, changes in expression of either the receptor or ligands of these signalling pathways are associated with pathophysiological conditions, including retinal vascular disorders (Akwii & Mikelis, 2021). Although, several anti-angiogenetic drugs have been approved that target the VEGF pathway for the treatment of ischemic retinopathies, most are anti-VEGF (Akwii & Mikelis, 2021; Tah et al., 2015). Studies on the molecular mechanisms and of the role of specific genes involved in pathological retinal NV are greatly facilitated by genetically modified mouse strains (Smith et al., 1994; Vähätupa et al., 2020). Therefore, understanding the processes behind retinal NV in the OIR model can help to identify new therapies for human NV retinal diseases (Scott & Fruttiger, 2009; Vähätupa et al., 2020).

1.6. **Transgenic mice**

Humans and mice have several genetic and pathophysiological similarities, therefore genetically engineered mouse models are a powerful tool for studying human disease and their associated molecular mechanisms (H. Kim et al., 2018). Production of transgenic mouse strains comprises the introduction of DNA into the mouse genome, which can be done by different methods. The DNA can be introduced into the genome by retroviral infection of mouse embryos, microinjection of DNA constructs into the pronucleus of fertilized oocytes or by manipulation of mouse embryonic stem cells. In the latter process, modified stem cells are microinjected into blastocysts, which are implanted into the uterus of a foster mother. The embryonic stem cells and the blastocyst are derived from mouse lines with different coat colors, resulting in a chimeric offspring that is then subsequently crossed and intercrossed until mutant homozygous mice are obtained. Another method for DNA insertion or modification is the clustered regularly interspaced short palindromic repeat (CRISPR)/Cas9 technology that has been used most recently to develop transgenic mice due to its high efficiency, simplicity, cost-effectiveness and low fetal toxicity. This nuclease system allows insertion of various mutations in different genes better resembling human diseases (Lampreht Tratar et al., 2018).

Transgenic mice can in principle be divided into models of either loss or gain of function. Loss of function mice are also known as knockout mice, in which a specific gene is deleted or silenced, while gain of function mice overexpress a specific gene. Recombinant mouse lines can further be classified as either constitutive, in which the target gene is permanently activated/inactivated in all cells of the animal, or conditional, in which knockout/knock-in of the gene can be regulated in a spatiotemporal manner (Lampreht Tratar et al., 2018). Reporter mouse models can also be used to observe the expression of a specific gene by inserting a reporter gene, such as *GFP* and *lacZ* (Lampreht Tratar et al., 2018; Payne et al., 2018).

The Cre-loxP mediated recombination system is a gene editing tool that allows the study and examination of specific gene functions (McLellan et al., 2017). Cre is a recombinase enzyme produced by the P1 bacteriophage that recognizes and binds to a 34 base pair (bp) sequence, the locus of crossing over (x) *(loxP*) sites (H. Kim et al., 2018; McLellan et al., 2017; Sternberg & Hamilton, 1981). The binding of a single Cre recombinase enzyme to two *loxP* sites in the same orientation, causes excision of the *loxP* flanked (floxed) DNA from the genome, leaving only a single *loxP* site (H. Kim et al., 2018; McLellan et al., 2017; Payne et al., 2018). Although, the Cre-loxP system is predominantly used for gene excision, it can also be adapted, by changing the orientation and location of the *loxP* sites, to induce inversion and translocation of DNA between two *loxP* sites (H. Kim et al., 2018). In addition, this system allows generation of conditional inducible mouse models, in which genetic gain or loss can be temporally and spatially regulated. This requires breeding of first, a genetically modified strains that carries a genetic locus with floxed DNA, with a second strain expressing the Cre enzyme under the control of a promoter and enhancer sequences that specifically targets cells or tissue of interest (H. Kim et al., 2018; McLellan et al., 2017).

Inducible systems enable the study of genes that are essential for development, in which constitutive knockout can lead to lethality or development defects. The most broadly used

inducible approaches are Cre fusion to a mutant estrogen receptor ligand binding domain (ER-LBD) and doxycycline (dox)-inducible Cre expression (H. Kim et al., 2018; McLellan et al., 2017). The Cre-ER recombinase, also known as CreERT2 or CreER^{T2}, is normally present in the cytoplasm where it binds to the heat shock protein 90 (HSP90), which prevents the Cre from entering the nucleus (H. Kim et al., 2018; McLellan et al., 2017; Payne et al., 2018). Tamoxifen or 4-hydroxytamoxifen are synthetic steroids administered systemically via intraperitoneal injection (IP) or gavage (H. Kim et al., 2018). Moreover, 4-hydroxytamoxifen can also be locally administrated. Tamoxifen leads to disruption of the interaction between HSP90 and CreERT2. This enables translocation of the CreERT2 to the nucleus and interaction of Cre with *loxP* sites (Figure 1.6) (H. Kim et al., 2018; McLellan et al., 2017; Payne et al., 2018). The dox-inducible Cre system, also called tetracycline (Tet) consists of three elements, reverse tetracycline-controlled transactivator (rtTA), tetracycline-controllled transactivator (tTA) and tetracycline operon (TetO). This system functions in two modes, Tet-on and Tet-off, permitting dox-dependent gene activation or inactivation (H. Kim et al., 2018; McLellan et al., 2017). Dox is normally administered in the food or drinking water (H. Kim et al., 2018). In the Tet-off system the tTA protein binds to the TetO promoter, thereby activating Cre expression. Dox administration inactivates the tTA protein that can no longer bind to TetO. In contrast, in Tet-on system *tTA* gene is replaced by *rtTA* genes, which only binds TetO in the presence of dox, thereby activating Cre expression (H. Kim et al., 2018; McLellan et al., 2017).

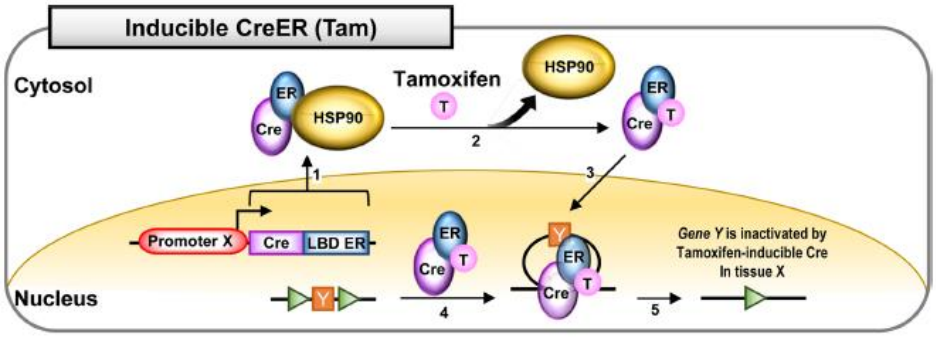

Figure 1.6. Tamoxifen inducible system consisting of estrogen receptor fused to Cre (CreER). In the absence of tamoxifen (Tam), the expressed fusion protein, CreER, interacts with HSP90 and exists in the cytoplasm. Administration of tamoxifen disrupts the interaction between HSP90 and CreER. Interaction of ER with tamoxifen induces the nuclear translocation of Cre. In the nucleus, the CreER recognizes the loxP sites and inactivates the gene Y in tissue X (adapted from H. Kim et al., 2018).

The Cre-loxP system is widely used due to its simple manipulation and efficient recombination. However, this system has some limitation that need to be taken into account when planning or analysing data from experiments. Specific promoters and enhancers that target a specific cell type can sometimes have off-target effects of Cre, therefore it is essential to evaluate cell-specific Cre expression in a newly generated Cre mouse line. The inducible Cre-loxP system can also lead to incomplete gene deletion of the floxed loci, which might depend on the recombination of the loci site or the method and frequency of tamoxifen administration. Another limitation of this system is the inability to analyse different cell types in an organ-specific manner (McLellan et al., 2017). Moreover, off-target effects of Cre expression can lead to potential toxicity of this system. Inducible cell-specific Cre expression toxicity has been

demonstrated in different tissues, including the mouse retina where tamoxifen-activated Cre-loxP system leads to impaired retinal angiogenesis independently of floxed target genes. Thus, tamoxifen-injected mice expressing Cre without floxed genes should be used as control in a study to assess possible Cre toxicity (Brash et al., 2020; McLellan et al., 2017).

In the vascular biology field, Cre activity is conventionally driven by an EC-specific promoter and enhancer that allows expression of the floxed gene in all ECs populations from early development. CreERT2 mouse models most used in vascular biology, where constitutive gene deletion often causes lethality, are *Cdh5-CreERT2* (VE-cadherin- CreERT2), *TEK-CreERT2* (Tie2- CreERT2) and *Pdgfb-CreERT2* (Payne et al., 2018).

1.7. *In vitro* models

The vascular system plays an important role in regulating homeostasis (Cochrane et al., 2019). Blood vessels display many differences depending on the tissue or organ with which they interact. In addition, different vascular beds from large arteries and veins to small post-capillary venules display distinct functions according to their size and vessel type (arteries or veins) (Cochrane et al., 2019; Sanz-Nogués & O'Brien, 2016). Vascular dysfunction can contribute to several pathological conditions, including cancer. The study of vascular function is essential to understand the molecular signalling pathways underlying vessels regulation in health and disease as well as for discovery of potential therapeutic targets and drugs (Cochrane et al., 2019).

Isolated ECs are used as *in vitro* models to study diverse physiologic and pathological processes, especially angiogenesis in which dysregulation is associated with several diseases, such as retinopathies (Cochrane et al., 2019; Krüger-Genge et al., 2019; Vähätupa et al., 2020). The *in vitro* culture models most commonly used are monolayer, transwell and pseudo-capillary. The transwell model is based on growth of ECs on a semipermeable membrane to allow the study of cell migration, transport or barrier function under a controlled gradient of solutes, while the pseudo-capillary model is used for analyses of microvascular capillary-like networks that form by seeding ECs on a soft hydrogel. In contrast, monolayers are simple 2D cultures models of ECs that enable analyses of molecular and cellular mechanisms, such as morphology, survival, migration, proliferation or barrier function (Cochrane et al., 2019). This model also allows to investigate the effect of drugs, inflammatory and pro- or anti-angiogenic factors on ECs.

In vitro models have a standard and well-controlled nature, which permits the systematic study of human cells under different experimental conditions (Cochrane et al., 2019). However, it is important to choose ECs that can better resemble the *in vivo* conditions under study (Sanz-Nogués & O'Brien, 2016). The best-characterized type of ECs used for *in vitro* analyses are human umbilical vein endothelial cells (HUVECs). These are primary, fully differentiated ECs, isolated from the umbilical cord after child birth. HUVECs are highly proliferative, robust in culture and prone to form capillaries (Kocherova et al., 2019; Sanz-Nogués & O'Brien, 2016). These cells also respond to diverse physiological and pathophysiological

stimuli and are easy to maintain in culture (Sanz-Nogués & O'Brien, 2016). However, although *in vitro* models are an important tool for assessing angiogenic and anti-angiogenic factors, validation of *in vitro* results by comparing with *in vivo* effects should be carry out.

2. MATERIALS AND METHODS

2.1. Antibodies

Retinal vasculature was immunostained with isolectin-B4 directly conjugated to Alexa647 (Invitrogen, 132450; 1/200). Phosphorylated VE-cadherin was stained with rabbit anti-phospho VE-cadherin Y685 (NEP-Precleaned pY685VEC; 1:100). Endothelial cells were stained with goat CD31 anti-rat (R&D Systems, AF3628; 1/500) or rat anti-mouse CD31 (BD Biosciences, 553370; 1/400) antibodies. Endothelial cell nuclei was stained with rabbit anti-Erg1/2/3 antibody (Abcam, ab92513; 1/500). Secondary conjugated antibodies used were donkey anti-goat Alexa488 (Invitrogen, A11055; 1/500), donkey anti-rabbit Alexa555 (Invitrogen, A31572; 1/500) and donkey anti-rat Alexa647 (Jackson ImmunoResearch, 712605150; 1/500).

HUVECs were stained with anti-rabbit PTPβ (or VE-PTP) (Santa Cruz Biotechnology, sc-28905; 1/100) antibody. Endothelial cell junctions were stained with goat anti-VE-cadherin antibody (R&D Systems, AF1002; 1/400). Secondary conjugated antibodies used were donkey anti-rabbit Alexa488 (Invitrogen, A21206; 1/500), donkey anti-goat Alexa555 (Invitrogen, A21432; 1/500) and Hoechst (Invitrogen, H3570; 1/2000).

For immunoblots analyses the following antibodies were used: rabbit anti-phospho VEGFR2 Y1175 (Cell Signalling, 2478; 1/1000), rabbit anti-VEGFR2 (Cell Signalling, 2479; 1/1000), rabbit anti-phospho Erk 1/2 pThr202/pY204 (Cell Signalling, 4377; 1/1000), rabbit anti-Erk 1/2 (Cell Signalling, 9102; 1/1000), anti-rabbit VE-PTP (HPA002700; 1/600), anti-rabbit VE-PTP (HPA054453; 1/600), anti-rabbit PTPRB (Invitrogen, PA5-68309; 1/1000), anti-rabbit PTPRB (Biorbyt, ORB317727; 1/1000) and an antibody against VE-PTP generated by immunizing rabbit with a peptide of VE-PTP (Storkbio; 1/500). Loading was normalized by blotting for mouse anti-GAPDH (glyceraldehyded-3-phosphatse dehydrogenase) (Sigma, MAB374; 1/2000). Horseradish peroxidase (HRP)-labelled secondary antibodies against mouse (NA931, from sheep) and rabbit (NA934, from donkey) were obtained from Cyvita (western blot, 1/10000).

2.2. Cell Culture

2.2.1. Human Umbilical Vein Endothelial Cells

Human umbilical vein ECs (HUVECs) (SclenCell) were cultured in tissue culture dish plates (Falcon) with EC basal medium MV2 (PromoCell) with all supplements (5% fetal calf serum, 5 ng/ml human epidermal growth factor (hEGF), 10 ng/ml human basic fibroblast growth factor (bFGF), 20 ng/ml insuline-like growth factor (R3 IGF-1), 0.5 ng/ml human VEGF, 1 µg/ml ascorbic acid and 0.2 µg/ml hydrocortisone) at 37°C in a humidified atmosphere containing 5% CO_2. Cells at 3 to 6 passages were used.

2.2.2. siRNA transfection

For small interfering RNA (siRNA)-mediated gene knock-down, HUVEC cells were seeded in 6-well plates at a density of 2.5×10^5 cells/well. After cells reached a 60-80% confluence, cells were changed to fresh medium 1 hour prior to transfection. HUVECs were transfected with 20 nM of siRNA targeting human *PTPRB* (EHU158501, Sigma) or scrambled non-silencing control siRNA (SIC001, Sigma), using 6 µl of Lipofectamine RNAiMAX (Invitrogen) in 300 µl of OptiMEM media (Gibco). Initially, to determine siRNA efficiency cells were transfected with different concentrations of siRNA (5 nM, 10 nM, 15 nM, 20 nM), keeping a 1:3 ratio of siRNA to lipofectamine. Culture medium was changed the day after transfection. Cells transfected for 48h were either washed once with 1xPBS (Gibco) and harvested for real-time quantitative polymerase chain reaction (RT-qPCR), or used for assays.

For study of VE-PTP junctional localization, round cover glasses were placed into a 6-well plate and coated with 0.1% of fibronectin from human plasma (Sigma) diluted 1/100 in 1x PBS. HUVECs were seeded and transfected with siRNA as described above or not. After 48 hours transfected cells were starved for 20 hours with MV2 medium with 0.5% fetal bovine serum (FBS) and without VEGF and bFGF supplements and fixed in 1% paraformaldehyde (PFA) for 15 minutes (min) at room temperature for immunofluorescence staining.

2.2.3. VEGFA stimulation assay

For signalling studies, 48 hours after transfection, HUVECs were starved for 2 hours in MV2 medium with 0.1% FBS (Gibco). After starvation, HUVECs in a 6-well plate were stimulated with recombinant murine VEGFA (50 ng/ml; PeproTech) in 600 µl of starving medium for the indicated duration. Cells were placed on ice, washed once with cold 1xPBS and lysed for 1 to 2 min using 100 µl of ice-cold radioimmunoprecipitation assay (RIPA) buffer (Invitrogen) with cOmplete protease inhibitor cocktail (Roche) (one tablet in 50 ml of lysis buffer), PhosSTOP phosphatase inhibitors (Roche) (one tablet for 10 ml of lysis buffer) and 1 mM of sodium orthovanadate (Na_2VO_4). Scrapped cells were harvested and centrifuged at 4°C, 21100xg for 5 min. The pellet was discarded and protein concentration was determined by Bradford assay using protein assay dye reagent concentrate (Bio-Rad). Bovine serum albumin (BSA) (Roche) was used as standard, protein samples were diluted 1/500 and concentrations

were determined by measuring absorbance at 595_{nm} using Synergy HTX multi-mode microplate reader (BioTex). The same amount of protein from each condition were used for immunoblotting analyses. Experiments were replicated three to four times for each condition.

2.3. Animal Studies

All mice husbandry, procedures and oxygen-induced retinopathy (OIR) challenge took place at Uppsala University, according to the 3Rs policy (Replacement, Reduction and Refinement) and the University board of animal experimentation approved all animal work for those studies (6789/18).

2.4. VE-PTP mouse model

VE-PTP floxed (Ptprbflox/ Ptprbtm2a (EUCOMM)Seq) (Figure 2.1) mouse line, originally generated by Susan Quaggin (Carota et al., 2019), on the genetic C57BL6/J background driven was used for *in vivo* studies. The mouse was crossed with Cdh5-CreERT2 mouse line to generate inducible endothelial specific *Ptprb* knockout. Cre activity and deletion of the floxed *Ptprb* alleles were induced postnatally by intraperitoneal (IP) injection of tamoxifen (Sigma) diluted in peanut oil (Sigma) at indicated amount and time points for each experiment. Animals were propagated at the local animal facility under laminar airflow conditions with 12 hours light/dark cycle at a temperature of 22-25°C. Animal housing and procedures were in accordance with animal welfare legislation and approved by the local animal ethics committees.

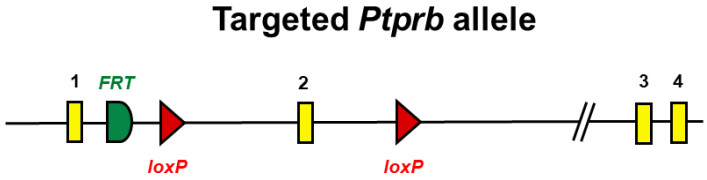

Figure 2.1. Floxed *Ptprb* exon 2 targeted to generate *Ptprb* inducible knock-out mice.

Ptprb inducible EC knock-out (iECKO) mice were genotyped by polymerase chain reaction (PCR), using genomic DNA from mouse toe (for pups) or ear clips. For DNA extraction, each tissue biopsy was boiled at 97°C for 30 min with 100 µl of alkaline solution (25 mM sodium hydroxide and 2 mM EDTA) and neutralized with 100 µl of 40 mM Tris-HCl pH 8 solution. PCR was performed using the following primers: *Ptprb*, forward 5´-GCGTCTATCCAGTGGAGGACTTTC-3´, reverse 5´-CCAGGTGCCGTTCATTCAGC-3´ (WT: 489 bp product; *Ptprb*: 546 bp); and Cre, forward 5´-GCCTGCATTACCGGTCGATGCAACGA-3´, reverse 5´-GTGGCAGATGGCGCGCGGCAACACCATT-3´ (~800 bp product). Each reaction mixture with a total volume of 20 µl was prepared using HotStartTaq Plus Master Mix Kit (Qiagen), containing 0.5 µl of 10 µM forward and reverse primer for a specific gene, 2 µl of 2x CoralLoad Concentrate, 10 µl of 2x HotStarTaq Plus Master Mix, 5 µl of RNase-free water and 2 µl of

DNA sample. PCR reaction was carried out in Applied Biosystems® Veriti 96-well Thermal Cycler with either Cre or *Ptprb* program shown in Table 2.1.

Table 2.1. PCR conditions for amplification of the *CRE* and *Ptprb* genes.

Cre			***Ptprb***		
Temperature	Time (min)	Number of cycles	Temperature	Time (min)	Number of cycles
95°C	5	-	94°C	5	-
95°C	0.30	40	94°C	0.30	35
55°C	0.30		62°C	0.30	
72°C	1.30		68°C	1.30	
72°C	5	-	68°C	5	-

PCR products were visualized on a 2% (w/v) agarose (Lonza) gel prepared in 1x TAE (Tris-acetate-EDTA) buffer (VWR life science). To each gel 1 µl/10 ml of SYBR® Safe DNA gel stain (Invitrogen) was added. Electrophoresis was performed at 130 V, 400 mA, 100 W for either 30 min or 1 hour and 15 min for *Cre* and *Ptprb* genes, respectively. Gels were imaged with trans-UV light on Chemidoc™ MP Imaging System (Bio-Rad). The 100 bp DNA ladder (Invitrogen) was used as reference to confirm the presence of Cre and *Ptprb* PCR products.

2.4.1. Vascular Development

Cre activity was induced on *Ptprb$^{fl/fl}$;Cdh5-CreERT2* pups (female and male) by IP injection of 100 µg or 400 µg of tamoxifen at P1, P2 and P3. Mice were sacrificed at P6 and eyes and lungs were collected. Eyes were fixed in 2% PFA for 1 hour at room temperature, washed three times for 10 min in 1xPBS and dissected for retina´s analyses. Lungs were either placed in RNAlater® solution (Sigma) for later RNA extraction or snap frozen in 2-methylbutane (Honeywell) with dry ice, immediately after collection. Snap frozen lungs were disrupted on ice in RIPA lyses buffer with inhibitors as described before (section 2.2.3) with the rotor tissue homogenizer Tissue-Tearor (Biospec Products). Lysates were centrifuged at 4°C, 21100xg for 10 min, the pellet was discarded and protein concentration was determined by Bradford assay as described on section 2.2.3 using a dilution of 1/2500. Protein was stored at -80°C.

2.4.2. Oxygen-induced retinopathy

A standard OIR model was used as described in Connor et al., 2009. In this procedure one litter of pups and their respective mother were placed into a chamber with an oxygen concentration of 75.0% (ProOx 110 sensor and A-Chamber, Biospherix, Parish, NY). Pups were weighed at P7 before entering the oxygen chamber. Mice remained in the chamber for 5 days, from P7 to P12, while lactating adult females were removed from the chamber on P8, P9, P10 and P11 for 2 hours a day. At P12 mice were returned to normal atmospheres (~21% oxygen), and IP injections of 400 µg of tamoxifen were given at P12, P13 and P14. At 17, pups were weighed and sacrificed by cervical dislocation along with their mother. Eyes from pups were immediately collected, fixed in 2% PFA at room temperature for 1 hour and washed 3 times with PBS for 10 min before retinas dissection.

2.5. Western Blot

Proteins obtained from cells and lung lysates were prepared according to NuPAGE (Invitrogen) instructions for reducing sample preparation. To each 15 µg and 150 µg of protein sample from cells and lung lysates, respectively, 5 µl of NuPAGE LDS Sample Buffer (4x), 2 µl of NuPAGE Sample Reducing Agent (10x) and Milli-Q water up to 13 µl were added. Samples were boiled at 70°C for 10 min to denature proteins. Proteins were separated on NuPAGE Novex 4-12% Bis-Tris polyacrylamide gel (Invitrogen) in running buffer (MOPS (1x) (Invitrogen) in deionized water) and reducing buffer (MOPS (1x), NuPAGE antioxidant). Electrophoresis was performed at 200 V, 400 mA, 100 W for 50 min. Separated proteins were transferred to a methanol (Supelco) pre-wetted polyvinylidene difluoride (PVDF) membrane (Invitrogen) in transfer buffer (NuPAGE transfer buffer (1x), 10% methanol and deionized water) and electrophoresis was executed at 30 V, 100 mA, 100 W for 1 hour and 30 min. Subsequently, membranes were blocked with 5% (w/v) skim milk (Semper) or 5% (w/v) BSA in Tris-buffered saline (1x) (G-Biosciences) with 0.1% Tween 20 (Sigma) (TBST) for 1 hour and 30 min, respectively. The membranes were incubated with primary antibodies overnight (ON) at 4°C and secondary antibodies linked to horseradish peroxidase (HRP) incubated for 1 hour at room temperature, diluted in either 5% milk or 5% BSA in TBST. After each step membranes were washed three times with TBST. HRP signals were visualized by enhanced chemiluminescence (ECL) detection kit (Amersham, Cytiva) and imaged with Chemidoc™ MP Imaging System (Bio-Rad). Immunoblots were stripped with stripping solution (2% SDS, 62.5 mM Tris-HCl pH 6.8 and 0.07% of β-mercaptoethanol) in a water bath at 50°C for 6 min, washed five times with TBST and blocked before new antibody incubation. Quantification of immunoblotting was performed on multiple replicate experiments using Image Lab software version 6.1 (Bio-Rad).

2.6. RNA isolation, cDNA synthesis and real-time quantitative PCR

Total RNA from HUVECs 48h after transfection and P6 mouse lungs was isolated using the RNeasy® Plus Mini Kit (Qiagen, Germany), following manufacturer's instructions. Extracted RNA concentration and purity absorbance ratios ($260_{nm}/280_{nm}$ and $260_{nm}/230_{nm}$) were measured on NanoDrop 2000 spectrophotometer (ThermoFisher Scientific). Complementary DNA (cDNA) was synthetized with 1 µg of RNA using reverse-transcription protocol from iSCRIPT advanced cDNA synthesis kit for RT-qPCR (Bio-Rad). Resulting cDNAs were diluted 1:5 in nuclease-free DEPC-treated water (Invitrogen).

For RT-qPCR, cDNAs were further diluted 1/9 and a master mix was prepared using SsoAdvanced Universal SYBR® Green Supermix (Bio-Rad) and 10 µM of desired forward and reverse primers. RT-qPCR was performed in a 96-well DNase/RNase free plate with the following conditions: pre-incubation at 95°C for 5 min; 39 amplification cycles at 95°C for 15 seconds and 60°C for 30 seconds; followed by a melting step at 60°C for 5 seconds with an increase in temperature of 0.5°C/cycle until reach 95°C. The housekeeping gene ribosomal protein L19 (*RPL19*) was used to normalize the mRNA expression levels of the target gene´s

analysed. The sequences of the gene-specific primers used are listed on Table 2.2. All primers were designed using Primer-BLAST online platform from NCBI (National Center for Biotechnology Information, U.S. National library of Medicine).

Table 2.2. Human (h) and Mouse (m) primer sequences used for RT-qPCR

Genes	Forward primer	Reverse primer
h*PTPRB*	5´-GCGGACCAGGATTCCCTCTA-3´	5´-AACTCCCGGATGGTCC-3´
h*RPL19*	5´-TCGCCTCTAGTGTCCTCCG-3´	5´- GCGGGCCAAGGTGTTTTTC-3´
m*Ptprb*	5´-GGGTCTCTAGCTTGTCAGCG-3´	5´-GACCTGCAGGGTGGTTGATG-3´
m*Rpl19*	5´-GGTGACCTGGATGAGAAGGA-3´	5´-TTCAGCTTGTGGATGTGCTC-3´
m*Flk1*	5´-CTACAGACCCGGCCAAACAA-3´	5´-CAGCTTGGATGACCAGCGTA-3´
m*Tie2*	5´-GCTCAGGCATTCCAGAACAGA-3´	5´-CCCTCTCCGATCACGTCTTG-3´
m*Cdh5*	5´-CACGGACAAGATCAGCTCCT-3´	5´-GGTAGCATGTTGGGGGTGTC-3´

2.7. **Immunofluorescent staining**

Dissected retinas fixed in 2% PFA were first blocked for 3 hr at room temperature under agitation in blocking buffer (3% BSA, 0.5% Triton X-100 (Sigma) in PBS, or 1% BSA, 0.25% Triton X-100 in PBS, for P6 and P17 retinas, respectively) to block unspecific binding. Incubation with the appropriate primary antibodies and secondary antibodies (diluted in buffer 1%BSA, 0.25% Triton X-100 in PBS), including Isolectin-B4 for P6 retinas, was performed sequentially over night at 4°C on a rocking platform, with three 1 hour washing steps with 0.25% Triton X-100 in PBS in between. After incubation with secondary antibodies, retinas were washed 2 times for 1 hour with 0.25% Triton X-100 in PBS, once with PBS for 30 min, post fixed with 4% PFA for 15 min (for P17 retinas), washed 3 times for 30 min with PBS and flat-mounted on slides with Fluormount-G mounting media (Southern Biotech) by cutting into 4 leafs.

Cells fixed in 1% PFA were washed twice in 1xPBS for 15 min and permeablized and blocked in 0.1% Triton X-100, 1% BSA in PBS for 1 hour at 37°C. Incubation with primary antibodies and secondary antibodies in 0.1% Triton X-100, 1% BSA in PBS was carried out sequentially, ON at 4°C and for 1 hour at room temperature, respectively. Cells were washed after each antibody incubation 3 times for 15 min or 5 min, respectively, with 1xPBS. Cells were mounted with Fluormount-G mounting media with 4´,6-diamidino-2-phenylindole (DAPI) (Southern Biotech).

Microscopy was performed on a Leica SP8 confocal microscope. Images were acquired with 20x and 40x objectives. Processing and quantification of images was done using ImageJ software (National Institutes of Health) to assess vascular density, vessel outgrowth and tip cell density on P6 retinas as well as avascular area and NV tufts area on P17 retinas after OIR experiment. Quantification of each image was performed blindly to sample´s genotype. All images shown are representative of images that were quantified.

2.8. Quantification of vessel density, tip cell density and outgrowth

Immunostaining for CD31, IB4 and ERG was performed on P6 retinas from tamoxifen treated *Ptprb*$^{fl/fl}$*;Cdh5-CreERT2* and *Ptprb*$^{fl/fl}$ mice and images were analysed using ImageJ software. Quantification of vessel density was performed manually by selecting all CD31 positive vessels using the threshold default parameter, creating a region of interest (ROI) for the vessel area of each whole mounted retina. Outgrowth was determined by measuring the length in µm from the optical nerve to the vessels front using the freehand lines tool. The average length of the four leafs of each flat-mounted retina was calculated and was represented has the outgrowth. For tip cell density quantification, CD31 and ERG composite images were used. For each retina leaf, the length of the vascular front was measured using the freehand line tool and tip cells number was counted. Tip cell number was normalized to the respective length and tip cell density was represented as the average tip cell number per length (µm) for a given retina.

2.9. Quantification of avascular area and neovascular tufts

Immunostaining for CD31 and VE-cadherin p-Y685 was performed on P17 retinas from OIR *Ptprb*$^{fl/fl}$*;Cdh5-CreERT2* and *Ptprb*$^{fl/fl}$ mice. Quantification of total vascularized area, central avascular area and tuft area was performed by outlining images manually in ImageJ software. For each whole mounted retina, the tile-scan of the CD31 channel and the polygon selection tool were used to demarcate the vascular front, creating a ROI for the vascularized area. Similarly, the avascular area was determined using the polygon selection tool to outline the central avascular region of the retina. The avascular area was normalized to the total vascularized area and was reported as a percentage of the total retina that was avascular. For tuft area quantification, the freehand selection tool was used to outline vessels from NV tufts (regions with disorganized dilated vessels). Tufts ROIs were summarized into a single ROI corresponding to the mean area of all NV tufts for a given retina. Tuft area was calculated by multiplying the mean tufts area by the number of selected tufts in each retina and normalize it to the total vascularized area. Tuft area was reported as the percentage of the total retina that contained tufts.

2.10. Statistical Analysis

Statistical analysis was performed with GraphPad Prism software (version 9.2.0). Unpaired Student´s *t*-test was used to compare two data sets, while multiple *t*-test was used for more data sets. All tests were two-tailed, parametric tests and p-value <0.05 was considered a statistically significant result. Quantitative phenotyping data and graphical representations were presented as means, with standard error of mean (SEM) used to describe the variability within the sample. For *in vivo* experiments 6 to 7 animals per experiment were used (detailed

number of animals used given in figure legends). For *in vitro* experiments 3 to 4 replicate experiments were used (detailed number in figure legends). Statistical significance is indicated as follows: *$p \leq 0.05$, **$p \leq 0.005$, ***$p \leq 0.0009$, ****$p < 0.0001$.

3. RESULTS

3.1. *PTPRB* is efficiently silenced after siRNA transfection

In order to identify specific antibodies against VE-PTP, first efficient silencing of its mRNA (denoted *PTPRB*) was determined by targeting human *PTPRB*. HUVEC cells were transfected with different concentrations (5 nM, 10 nM, 15 nM and 20 nM) of control siRNA or *PTPRB* siRNA, and a lipofectamine control was used to assess possible cytotoxic effects. At 48 hours after transfection, RNA was isolated from the cells and RT-qPCR was performed. The RT-qPCR showed approximately a 40% reduction in *PTPRB* expression levels upon 20 nM siRNA transfection for 48 hours, compared to the respective control treated cells (Figure 3.1). Lipofectamine at this concentration had no significant cytotoxic effect on cells. Lower concentrations of siRNA were unable to reduce *PTPRB* expression by more than 20% (Figure 3.1). Thus, 20 nM of *PTPRB* siRNA was determined as the working concentration for efficient silencing of *PTPRB*.

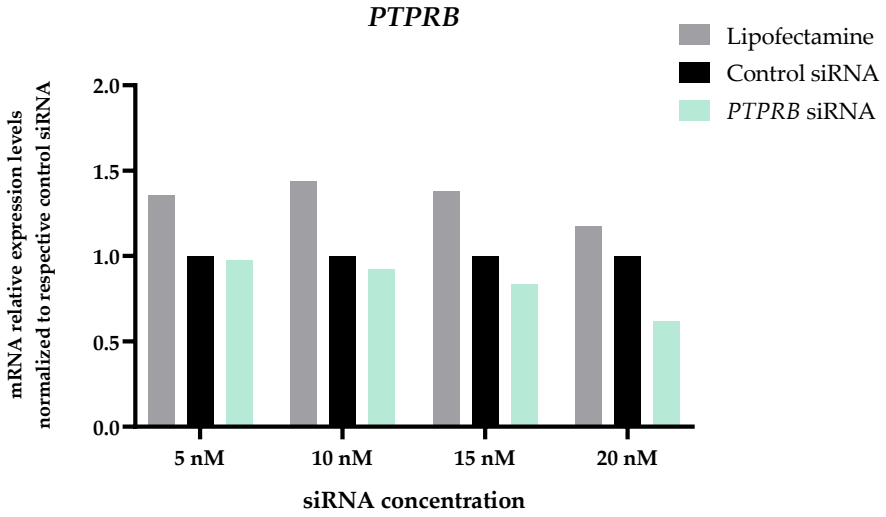

Figure 3.1. *PTPRB* expression levels in siRNA transfected HUVECs. RNA was isolated from HUVECs either transfected with 5 nM, 10 nM, 15 nM or 20 nM of siRNA targeting human *PTPRB* or control siRNA, or treated with lipofectamine. cDNA was obtained by reverse transcription and RT-qPCR was performed. *PTPRB* relative expression levels were normalized to *RPL19* expression levels and transcript levels were further normalized to the respective control siRNA treated sample. Results represent relative ratios between mRNA expression levels of *PTPRB* and *RPL19*. Data from triplicates is represented.

3.2. Identification of VE-PTP specific antibodies

Given the results obtained from *PTPRB* expression analyses of siRNA transfected samples, we decided to identify and evaluate the specificity of several VE-PTP antibodies. Immunoblotting with custom-produced and commercially available antibodies against human VE-PTP was performed on protein samples from HUVECs treated with lipofectamine or transfected with 20 nM of *PTPRB* or control siRNAs and cell lysates, harvested after 48 hours. First, we assessed the specificity of the antibodies for human VE-PTP by detecting two prominent bands at a molecular weight of ~240 kDa and ~260 kDa, in agreement with the appearance of VE-PTP upon immunoblotting described in a previous report (Nawroth et al., 2002). The lower band assumed to represent VE-PTP was fainter than the upper band and it was sometimes difficult to detect in immunoblots (Figure 3.2). *PTPRB* silencing allowed confirmation of antibody specificity for the VE-PTP protein. As shown in Figure 3.2, *PTPRB* silencing reduced VE-PTP band intensity compared to control or lipofectamine samples on immunoblots with Storkbio, HPA054453 and HPA002700 antibodies. However, protein levels in the silenced *PTPRB* samples were similar to the control samples in immunoblots using Invitrogen and Biorbyt antibodies (Figure 3.2). Quantification of the immunoblots further confirmed the specificity of Storkbio, HPA054453 and HPA002700 antibodies to human VE-PTP (Figure 3.3).

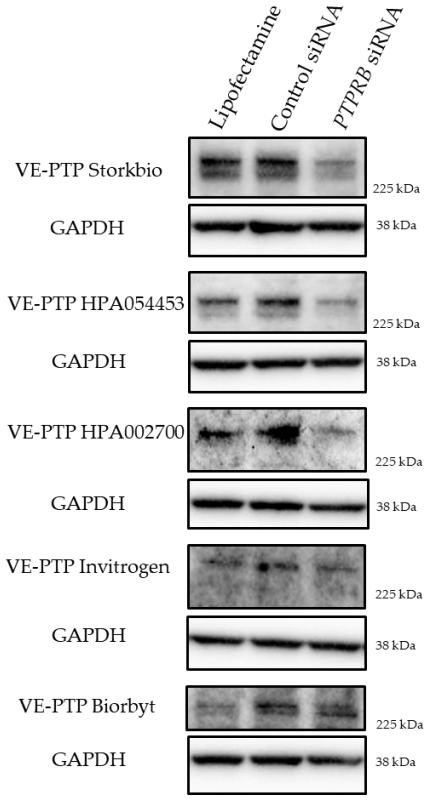

Figure 3.2. Antibody specificity for human VE-PTP. HUVECs were treated either with lipofectamine alone, or combined with control siRNA or *PTPRB* siRNA for 48 hours at a concentration of 20 nM. Cells lysates were subjected to immunoblotting with several antibodies reacting with VE-PTP: Storkbio, HPA054453, HPA002700, Invitrogen and Biorbyt. Blotting for GAPDH shows equal loading of the lysates. Molecular weights are shown to the right in the blots. Western blots were analysed for the presence of specific VE-PTP bands (~240 and 260 kDa) and for reduced VE-PTP band intensity upon *PTPRB* silencing compared to controls. Quantification of immunoblots VE-PTP/GAPDH levels provided in Figure 3.3.

Due to the availability and specificity of the HPA054453 antibody for human VE-PTP, we decided to use it for subsequent immunoblots analyses. Although RT-qPCR data showed a 40% reduction of *PTPRB* transcript level, in western blot quantification a 50-60% reduction in VE-PTP proteins levels upon *PTPRB* silencing compared to control siRNA treated cells was observed (Figure 3.3). This further supports the specificity of the HPA054453 antibody for the human VE-PTP protein.

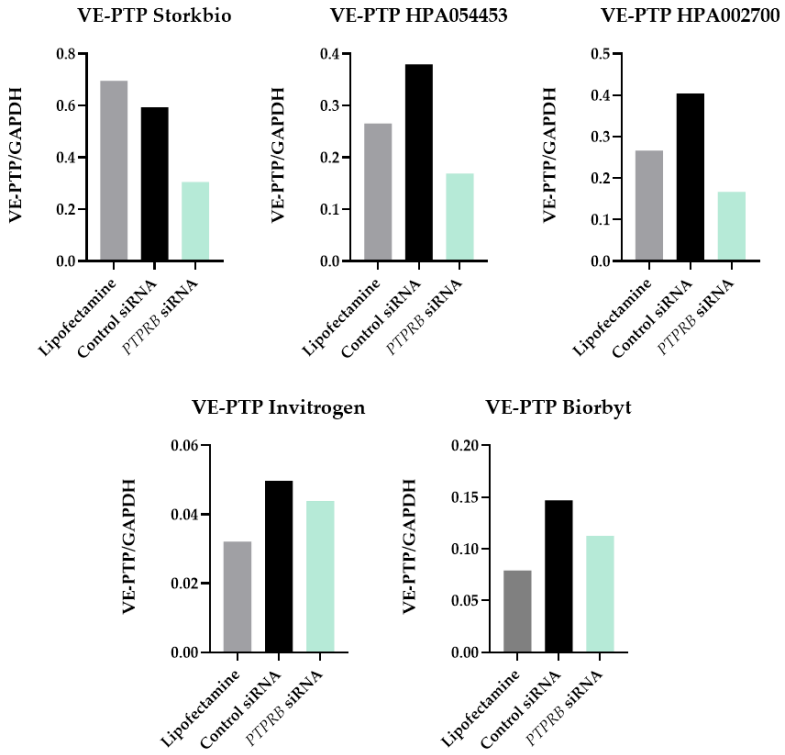

Figure 3.3. Immunoblots quantification of VE-PTP protein levels for determination of antibody specificity. HUVECs were treated either with lipofectamine, or control siRNA or *PTPRB* siRNA for 48 hours at a concentration of 20 nM. Cells lysates were subjected to immunoblotting with several antibodies reacting to VE-PTP: Storkbio, HPA054453, HPA002700, Invitrogen and Biorbyt. Quantification of VE-PTP/GAPDH levels for each VE-PTP antibody tested is representative of one experiment. Antibody specificity was assessed based on the degree of reduction of VE-PTP/GAPDH levels in *PTPRB*-deficient cells compared to controls. Specificity for human VE-PTP was verified in blots probed for VE-PTP with Storkbio, HPA054453 and HPA002700 antibodies.

3.3. VE-PTP localizes to endothelial cell junctions

VE-PTP was previously described to localize at endothelial cell contacts of confluent mouse bEnd.3 endothelioma cells (Nottebaum et al., 2008). To assess whether the same could also be verified in HUVECs, immunostaining for VE-PTP and VE-cadherin was performed. For this purpose, HUVECs were either untreated, or transfected with *PTPRB* siRNA or control siRNA and starved for 20 hours after transfection. The nuclei and EC junctions of confluent cells were stained for DAPI or Hoechst and VE-cadherin, respectively. The results showed regions of VE-PTP immunostaining overlapping with VE-cadherin immunostaining on untreated and siRNA control treated cells (Figure 3.4, arrows). In contrast, VE-PTP was not detected in *PTPRB* siRNA treated cells. Distribution of VE-cadherin protein was unaffected by *PTPRB* silencing. These data demonstrates that VE-PTP localizes at endothelial cell junctions of confluent ECs.

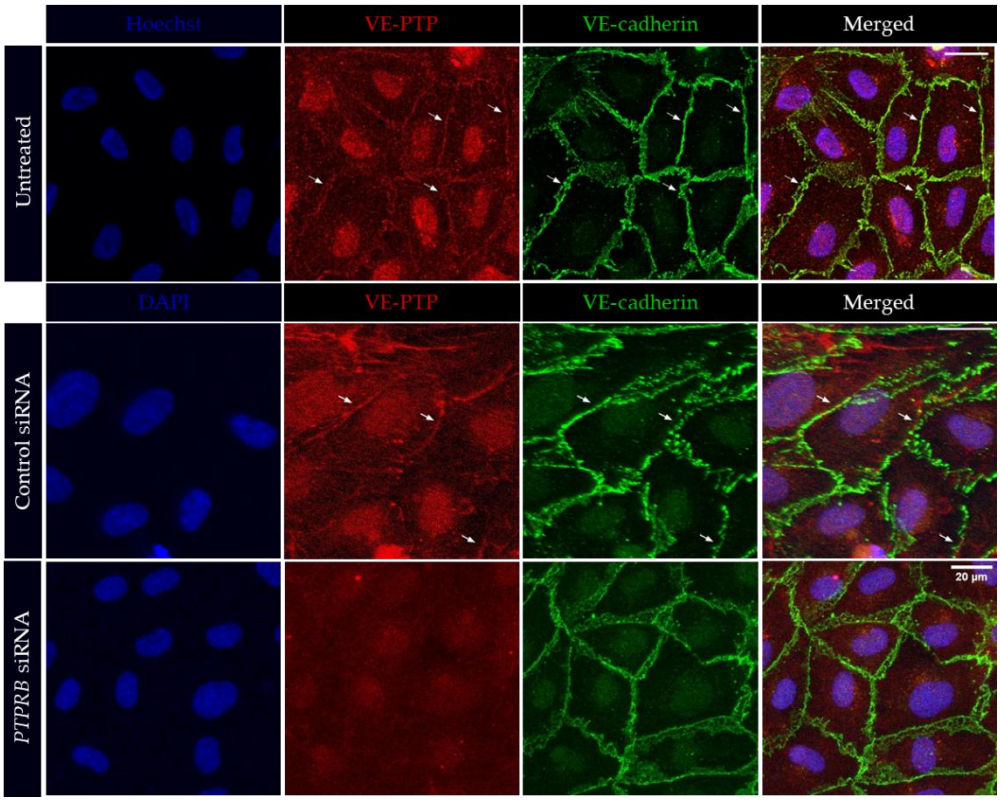

Figure 3.4. VE-PTP colocalizes with VE-cadherin at EC junctions. HUVECs either untreated or transfected with 20 nM of *PTPRB* siRNA or control siRNA for 48 hours were starved for 20 hours and immunostained for VE-PTP and VE-cadherin. Representative immunofluorescence images of the cells are shown: blue; DAPI or Hoechst 33342, red; VE-PTP, green; VE-cadherin/cell junctions. Arrows indicate colocalization between VE-PTP and VE-cadherin signals. Scale bar, 20 µm.

3.4. VEGFR2 phosphorylation at phosphosite Y1175 increases upon *PTPRB* silencing in VEGFA stimulated cells

To determine if *PTPRB* silencing affected VEGFR2 activity, the effect of *PTPRB* silencing on tyrosine phosphorylation at the Y1175 residue in VEGFR2 was studied. For this, HUVECs transfected with either *PTPRB* siRNA or control siRNA were stimulated without (0 min) or with VEGFA for 2 min, 5 min, 10 min, 15 min, 30 min, 60 min, 120 min, 240 min and ON. Cell lysates were used for western blot analyses. As shown in Figure 3.5, VEGFA stimulation of HUVECs induced an initial increase in tyrosine phosphorylation of VEGFR2 at Y1175, followed by a decrease after 5 minutes. In agreement with previous findings (Hayashi et al., 2013; Mellberg et al., 2009), the degree of phosphorylation increased further in VEGFA-stimulated cells treated with *PTPRB* siRNA (Figure 3.5). The total VEGFR2 levels were unchanged in the different conditions (Figure 3.5). These data shows that *PTPRB* silencing results in exaggerated VEGFA-induced VEGFR2 tyrosine phosphorylation, which returns with time to its basal levels.

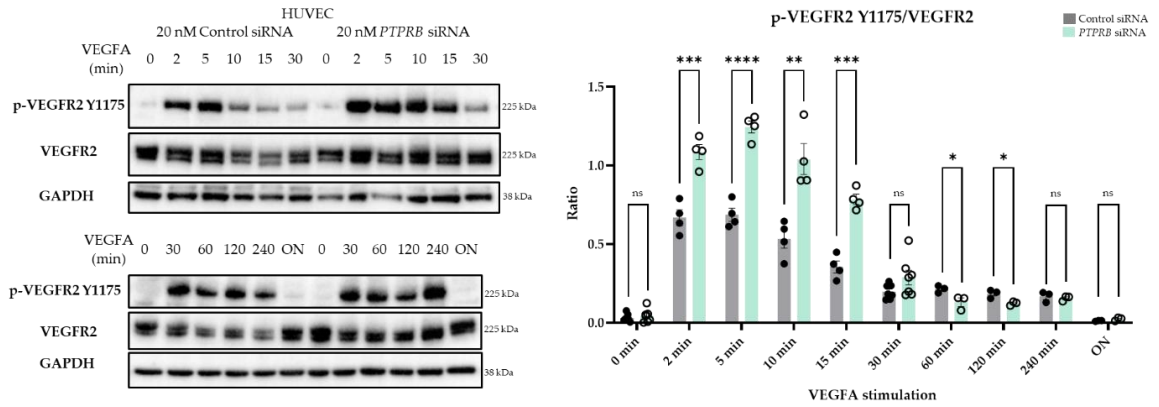

Figure 3.5. *PTPRB* silencing increases VEGFA-induced VEGFR2 phosphorylation at Y1175. HUVECs transfected with 20 nM of either control siRNA or *PTPRB* siRNA for 48 hours were treated without (basal) or with VEGFA (50 ng/ml) for the time points indicated. Analyses was performed by immunoblotting on total cell lysates. Representative blots are shown (left). Blots were probed for phosphorylated (p) VEGFR2 Y1175 and total VEGFR2. Blotting for GAPDH shows equal loading of the lysates. Molecular weights are shown to the right in the blots. Quantification of p-VEGFR2/VEGFR2 levels from four independent experiments (right). Values are means ± SEM. Student´s *t*-test; ns, not significant, *, p≤0.05, **, *p*≤0.005, ***, p≤0.0009, ****, *p*<0.0001.

3.5. Erk 1/2 phosphorylation decreases upon *PTPRB* silencing in VEGFA stimulated cells

To assess whether *PTPRB* silencing affected the signalling pathway downstream of VEGFR2, immunoblotting for extracellular regulated kinase (Erk) 1/2 was performed on total cell lysates previously used to examine VEGFR2 phosphorylation at Y1175. The serine/threonine kinases Erk 1/2 are essential in regulation of cell proliferation (Guo et al., 2020). As shown in Figure 3.6, a short stimulation with VEGFA induced phosphorylation of Erk 1/2, followed by a decrease after 10 min. Unexpectedly, VEGFA stimulation after *PTPRB* silencing reduced Erk 1/2 phosphorylation levels compared to control samples (Figure 3.6). The total Erk 1/2 levels were unchanged in the different conditions (Figure 3.6). Thus, although *PTPRB* ablation increased VEGFR2 phosphorylation at Y1175, Erk 1/2 signalling appeared to be negatively affected by the loss of *PTPRB* expression upon stimulation with VEGFA.

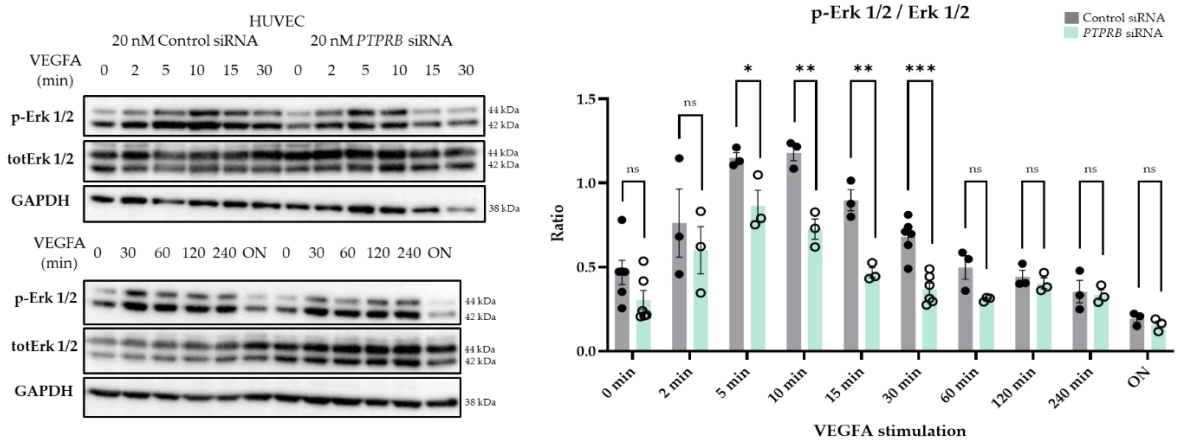

Figure 3.6. *PTPRB* silencing decreases VEGFA-induced Erk 1/2 phosphorylation. HUVECs transfected with 20 nM of either control siRNA or *PTPRB* siRNA for 48 hours were treated without (basal) or with VEGFA (50 ng/ml) for the time points indicated. Analyses was performed by immunoblotting on total cell lysates. Representative blots are shown (left). Blots were probed for phosphorylated (p) Erk 1/2 and total Erk 1/2. Blotting for GAPDH

shows equal loading of the lysates. Molecular weights are shown to the right in the blots. Quantification of p-Erk/total Erk levels from three independent experiments (right). Values are means ± SEM. Student´s *t*-test; ns, not significant, *, $p<0.05$, **, $p<0.005$, ***, $p\leq0.0003$.

3.6. *Ptprb* is efficiently deleted in *Ptprb$^{fl/fl}$;Cdh5-CreERT2* mice upon tamoxifen treatment

In order to examine the *in vivo* effect of *Ptprb* gene ablation and to bypass the embryonic lethality observed in constitutive *Ptprb* KO mice, an inducible endothelial cell KO (iECKO) mouse model was used. First, Cre-loxP system recombination efficiency was determined to ensure complete deletion of the floxed *Ptprb* gene. Cre activity was induced in *Ptprb$^{fl/fl}$;Cdh5-CreERT2* pups by IP injection of 400 µg of tamoxifen at P1, P2 and P3. Lungs were collected at P6 for protein and mRNA extraction and used for western blot and RT-qPCR analyses, respectively. The RT-qPCR showed that using this system, 97.7 ± 0.03% deletion efficiency of *Ptprb* was achieved following Cre induction compared to control littermates (Figure 3.7A). Immunoblots of lung lysates showed loss of most of the VE-PTP protein following Cre-induced gene ablation (Figure 3.7B), which further corroborates efficient gene deletion. Overall, these data shows efficient *Ptprb* deletion following tamoxifen injection and induction of Cre activity.

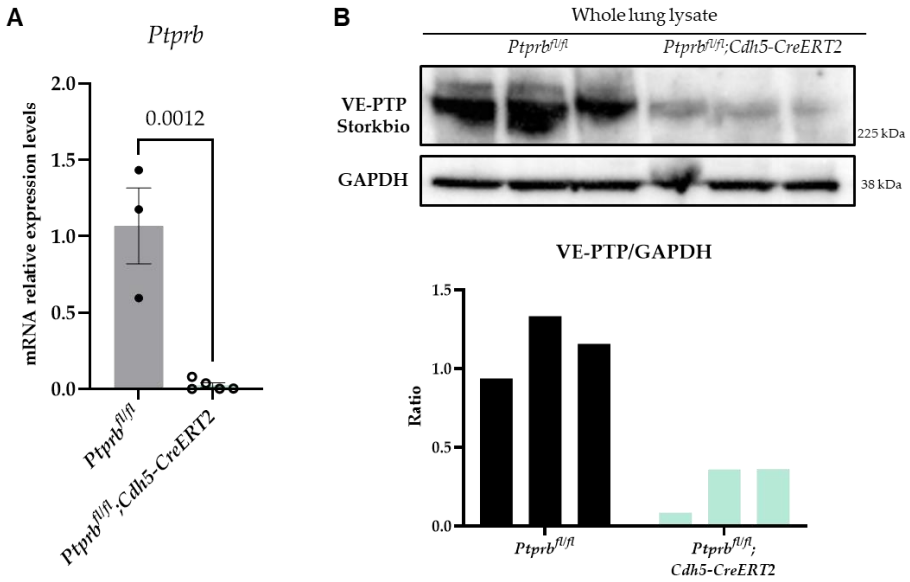

Figure 3.7. *Ptprb* is efficiently deleted in *Ptprb$^{fl/fl}$;Cdh5-CreERT2* mice. Lungs from P6 *Ptprb$^{fl/fl}$;Cdh5-CreERT2* or *Ptprb$^{fl/fl}$* pups treated at P1, P2 and P3 with 400 µg of tamoxifen were extracted and *Ptprb* knockdown was assessed by RT-qPCR and western blot. **(A)** Postnatal deletion of *Ptprb* in *Ptprb* iECKO mice leads to reduction of *Ptprb* mRNA expression levels (n=5 *Ptprb$^{fl/fl}$;Cdh5-CreERT2*; n=3 *Ptprb$^{fl/fl}$*; where n is the number of mice). Values are means ± SEM, with individual data points indicated. Statistical significance was determined using Student´s *t*-test, $p=0.0012$. **(B)** Immunoblot and quantification of VE-PTP/GAPDH levels from a single experiment is represented showing reduction in VE-PTP protein in total lung lysates from *Ptprb$^{fl/fl}$;Cdh5-CreERT2* mice compared with *Ptprb$^{fl/fl}$* (n=3/genotype, where n is the number of mice).

3.7. *Ptprb* iECKO impairs retina vascular development

During early postnatal development, retina endothelial cells proliferate and migrate in a VEGF/VEGFR2-dependent manner (Gerhardt et al., 2003). Therefore, to understand the EC-

specific role of VE-PTP during retinal vascular development, *Ptprb* iECKO mice were treated postnatally with tamoxifen to induce specific deletion of *Ptprb* (Figure 3.8A). Retinas from P6 mice were isolated and flat mounted for immunofluorescence analyses. Retina ECs were detected by immunostaining for CD31 and IB4 binding and EC nuclei were visualized by Erg immunostaining (Figure 5.1, in appendix). As shown in Figure 3.8B-C, the total vascular area, vessel outgrowth measured from the optic nerve and tip cell density were all reduced in *Ptprb$^{fl/fl}$;Cdh5-CreERT2* mice compared to control littermates. This suggests that VE-PTP might be required for regulation of VEGFR2 signalling and normal retina vascular development.

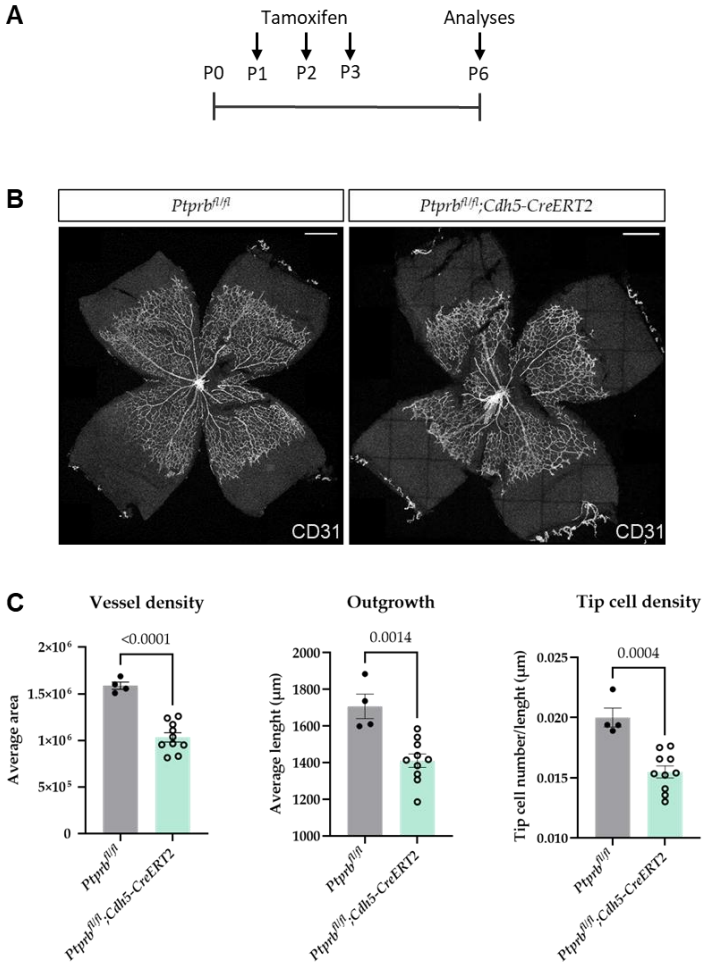

Figure 3.8. VE-PTP is required for retinal vascular development. Eyes from P6 *Ptprb$^{fl/fl}$;Cdh5-CreERT2* or *Ptprb$^{fl/fl}$* pups treated at P1, P2 and P3 with 100 µg of tamoxifen were used for immunofluorescence analyses. **(A)** Schematic of tamoxifen-induced *Ptprb* gene deletion strategy. **(B)** Representative images of the vasculature of whole mount P6 retinas from *Ptprb$^{fl/fl}$* and *Ptprb$^{fl/fl}$;Cdh5-CreERT2* mice immunostained for CD31. Scale bar, 500 µm. **(C)** Retina quantification is presented showing reduced vessel density (p<0.0001), reduced outgrowth from the optic nerve (p=0.0014) and lower tip cell density (p=0.0004) in *Ptprb* deficient mice (n=14, where n is the number of retinas). Data are means ± SEM. Values are either the representation of one or two retinas per mice. Statistical significance was determined using Student´s *t*-test (n=6 *Ptprb$^{fl/fl}$;Cdh5-CreERT2*; n=2 *Ptprb$^{fl/fl}$*; where is the number of mice).

3.8. *Ptprb* iECKO has no effect on *Flk1*, *Tie2* and *Cdh5* expression levels

VE-PTP is known to be specifically expressed on endothelial cells where it directly interacts with its substrates, VEGFR2, VE-cadherin and Tie2 (Bäumer et al., 2006; Vestweber,

2021). To determine whether *Ptprb* gene deletion was associated with changes in the expression levels of *Flk1* (VEGFR2), *Tie2* (Tie2) or *Cdh5* (VE-cadherin), we performed RT-qPCR analyses. For this purpose, lungs were harvested from P6 *Ptprb*$^{fl/fl}$;*Cdh5-CreERT2* and *Ptprb*$^{fl/fl}$ mice treated with tamoxifen and RNA was isolated for RT-qPCR. Similar to the results obtained on *Ptprb* floxing efficiency for P6 mouse lungs (Figure 3.7A), the mRNA expression levels of *Ptprb* were reduced in *Ptprb*$^{fl/fl}$;*Cdh5-CreERT2* mice after tamoxifen treatment (Figure 3.9). However, reduction of *Ptprb* expression had no effect on *Flk1*, *Tie2* and *Cdh5* expression levels (Figure 3.9). Although, there was a trend for a slight decrease in mRNA expression levels of *Flk1* and *Tie2* in *Ptprb*-deficient mouse lungs, this did not reach significant differences.

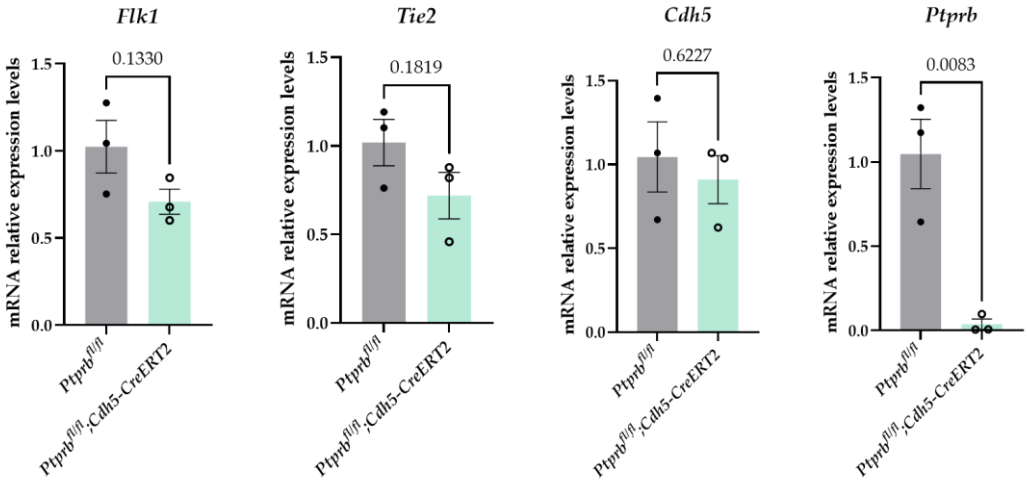

Figure 3.9. Expression levels of *Flk1*, *Tie2*, *Cdh5* and *Ptprb* on *Ptprb* iECKO mice. Lungs from P6 *Ptprb*$^{fl/fl}$;*Cdh5-CreERT2* or *Ptprb*$^{fl/fl}$ pups treated at P1, P2 and P3 with 400 µg of tamoxifen were harvested and *Flk1*, *Tie2*, *Cdh5* and *Ptprb* expression levels were assessed by RT-qPCR. Postnatal deletion of *Ptprb* led to reduction of *Ptprb* mRNA expression levels, but did not significantly affect expression levels of *Flk1*, *Tie2* and *Cdh5*. Values are means ± SEM, with individual data points indicated (n=3/genotype, where n is the number of mice). Statistical significance was determined using Student´s *t*-test.

3.9. *Ptprb* iECKO reduces vaso-obliteration in OIR mice

Pathological retinal neovascularization is triggered by increased VEGFA expression induced in hypoxia, which is characteristic of ischemic diseases, such as retinopathy of prematurity (Dai et al., 2021). Since VE-PTP was identified to have a role in regulating VEGFA/VEGFR2 signalling, we wanted to determine whether VE-PTP affected pathological retinal angiogenesis. The OIR mouse model was used to trigger vaso-obliteration and pathological angiogenesis (Connor et al., 2009). Briefly, *Ptprb*$^{fl/fl}$;*Cdh5-CreERT2* pups and their control littermates (*Ptprb*$^{fl/fl}$) were exposed to hyperoxia from P7 to P12. At P12, pups were returned to normoxic conditions and *Ptprb* gene deletion was induced by IP injection of tamoxifen at P12, P13 and P14. Eyes from P17 mice were collected and retinas were used for immunofluorescence analyses (Figure 3.10A). Retina vasculature was visualized by immunostaining for CD31 (Figure 3.10B). We observed decreased avascular area in *Ptprb*$^{fl/fl}$;*Cdh5-CreERT2* compared to the control littermates after exposure to hyperoxia (Figure 3.10C). However,

Ptprb ablation did not affect NV tuft area and number (Figure 3.10D-E). Although, there was a tendency for increase tuft number on *Ptprb*$^{fl/fl}$;*Cdh5-CreERT2* mice, it was not statistically significant. Of note, the morphology of the NV tufts in *Ptprb*$^{fl/fl}$;*Cdh5-CreERT2* retinas appeared distinct from that of the *Ptprb*$^{fl/fl}$ controls (see Discussion). This suggests a potential role for VE-PTP in retinal pathologies.

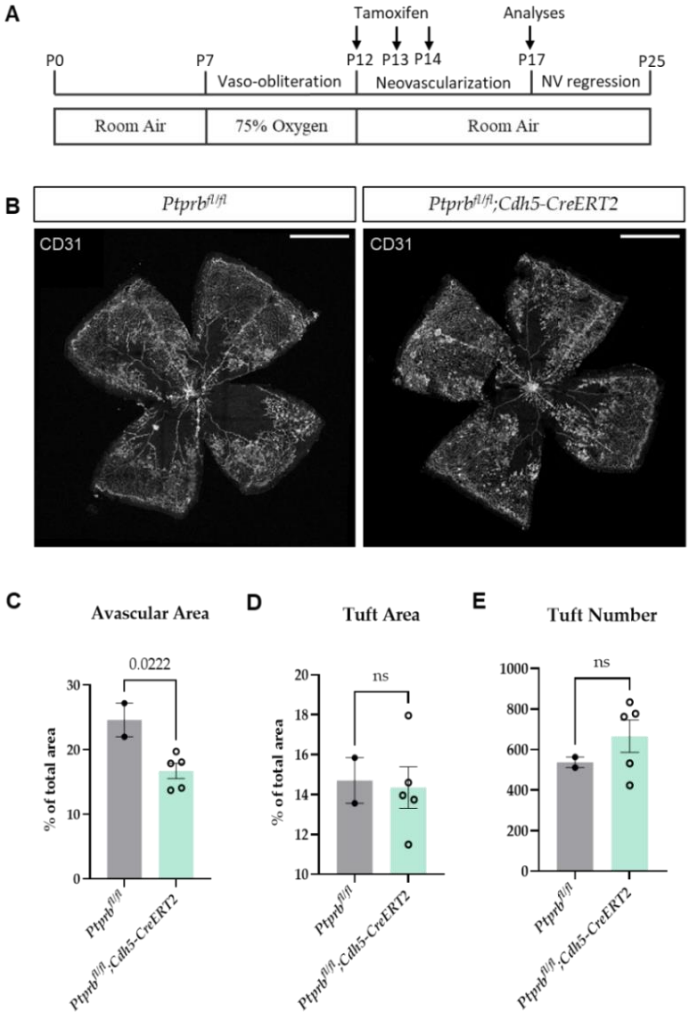

Figure 3.10. *Ptprb* deletion reduces vaso-obliteration in OIR mice. Retinas from *Ptrpb*$^{fl/fl}$;*Cdh5-CreERT2* or *Ptprb*$^{fl/fl}$ mice submitted to OIR challenge and treated at P12, P13 and P14 with 400 µg of tamoxifen were collected at P17 and used for immunofluorescence analyses. **(A)** Schematic of OIR strategy. **(B)** Representative images of whole mount retinas from *Ptprb*$^{fl/fl}$ and *Ptprb*$^{fl/fl}$;*Cdh5-CreERT2* mice, collected at P17 after OIR challenge, and stained with CD31 antibodies. Avascular tissue can be observed in the central retina and neovascular tufts, clusters of disorganized vessels, can be better observed in Figure 5.2, in appendix. Scale bar, 1000 µm. **(C)** Quantification of avascular area as a percentage of total retina area showing reduced avascular area in *Ptprb*$^{fl/fl}$;*Cdh5-CreERT2* compared to *Ptprb*$^{fl/fl}$ mice (p=0.0222). **(D)** Quantification of neovascular tuft coverage as percentage of total retina area. **(E)** Quantification of neovascular tuft number per retina. Data are means ± SEM. (n=5 *Ptprb*$^{fl/fl}$;*Cdh5-CreERT2*; n=2 *Ptprb*$^{fl/fl}$; where n is the number of mice). One retina per mouse was analysed. Statistical significance was determined using Student´s *t*-test.

4. Discussion

Activation of VEGFR2 signalling by VEGFA plays a key role in several physiological processes, such as in vascular permeability and angiogenesis (Corti & Simons, 2017). Several studies have shown that increased VEGFA expression and thereby activation of VEGFR2 signalling is a process that occurs in retinal diseases, such as in retinopathy of prematurity and age-related macular degeneration, and it is associated with increased vascular permeability and disease progression (Claesson-Welsh, 2015). The current ophthalmological therapies target the VEGF/VEGFR2 pathway to promote normalization of vessel function and structure (Akwii & Mikelis, 2021; Ferrara & Adamis, 2016). However, there are limitations of anti-VEGF therapies, as they require repeated administrations and patients may exhibit or acquire resistance to the angiogenic inhibitors. In certain cases, the therapies may have toxic side effects. Therefore, there is a need for new clinical treatments (Akwii & Mikelis, 2021; Carmeliet & Jain, 2011; Claesson-Welsh, 2015). Deeper understanding of the molecular mechanism underlying angiogenesis and permeability may provide new strategies to delay disease progression or improve treatment effectiveness and quality of life for patients with retinopathies.

VE-PTP is an endothelial specific tyrosine phosphatase that interacts with VEGFR2 and Tie2 on endothelial cells, thereby regulating their activity (Vestweber, 2021). Deletion of *Ptprb*, *Kdr* (VEGFR2) or *Tie2* leads to embryonic lethality in mice due to defects in vascular development (Bäumer et al., 2006; Eklund & Olsen, 2006; Shalaby et al., 1995). Furthermore, inhibition of VE-PTP in a disease mouse model of age-related macular degeneration was shown to strongly supress neovascularization by inducing Tie2 activity (Shen et al., 2014), suggesting a role for VE-PTP in disease outcome. Here we studied VE-PTP´s effect on VEGFR2 signalling and in an ischemic retinopathy mouse model to assess the potential therapeutic impact of targeting this molecule.

To perform the *in vitro* assays presented in this study, we first determined the efficiency of suppressing *PTPRB* expression by transfecting HUVECs with siRNA targeting *PTPRB* transcripts. RT-qPCR and immunoblots quantification for human VE-PTP showed consistent *PTPRB* silencing upon transfection with 20 nM of *PTPRB* siRNA for 48h (Figure 3.1). Higher concentrations of siRNA to improve even further suppression of *PTPRB* expression were not used due to potential lipofectamine cytotoxicity, which could compromise cell viability for subsequent experiments. Immunoblotting of cells lysates transfected with control or *PTPRB*

siRNA with several commercially available or custom-made VE-PTP antibodies against human VE-PTP, revealed that only the HPA002700 and HPA054453 commercial VE-PTP antibodies and the Storkbio custom-made antibody specifically recognizes the human VE-PTP protein (Figure 3.2). Moreover, efficient tamoxifen activation of Cre activity and subsequent *Ptprb* gene deletion in *Ptprb*$^{fl/fl}$;*Cdh5*-CreERT2 mice was observed on RT-qPCR for *Ptprb* (Figure 3.7A) and on whole lung lysates blotted with the Storkbio antibody (Figure 3.7B), which was generated to specifically target mouse VE-PTP protein.

VE-PTP has been shown to interact with VE-cadherin, Tie2 and VEGFR2 at EC-cell junctions (Fachinger et al., 1999; Mellberg et al., 2009; Nawroth et al., 2002). Immunostaining of HUVECs indeed showed preferential localization of VE-PTP at cell-cell junctions (Figure 3.4). Accordingly, VE-PTP staining was not observed upon deletion of *PTPRB* (Figure 3.4). This is in agreement with previous studies, were VE-PTP was found to translocate and localize to EC contacts in cultures with matured cell junctions (Hayashi et al., 2013; Nottebaum et al., 2008). VE-PTP staining observed at the nucleus of untreated and *PTPRB* siRNA-treated HUVECs (Figure 3.4), might be due to unspecific signals in immunofluorescence or VE-PTP localization within intracellular compartments, which occurs in recently confluent cultures (Nottebaum et al., 2008). Moreover, the distribution of VE-cadherin was unaffected by *PTPRB* silencing, in agreement with previous reports (Nottebaum et al., 2008).

VE-PTP is known to increase phosphorylation of VEGFR2 at Y1175 upon short stimulation with VEGFA (Hayashi et al., 2013; Mellberg et al., 2009). We showed in immunoblots of cells treated with control or *PTPRB* siRNA that *PTPRB* deficiency increases VEGFA-induced VEGFR2 phosphorylation at Y1175 (Figure 4.1), which resumes with time to its basal levels (Figure 3.5). This is in agreement with reported loss of VEGFR2/VE-PTP complex upon VEGFA stimulation and subsequent increase in VEGFR2 phosphorylation at Y1175, which also resumes with time to the levels observed in resting cells (Mellberg et al., 2009).

In Mellberg et al., *PTPRB* silencing in telomerase-immortalized human microvascular endothelial (TIME) cells affected downstream signalling transducers, leading to increased p-Akt and p-Erk 1/2 levels in unstimulated cells and a slight increase in p-Akt in response to VEGFA stimulation for 5 minutes. In contrast, we show that *PTPRB* silencing had no effect on Erk 1/2 phosphorylation in unstimulated HUVECs (Figure 3.6) and that Erk 1/2 phosphorylation consistently was lower after *PTPRB* silencing, in response to VEGFA treatment for up to 1 hour (Figure 4.1). The differences observed in Erk 1/2 phosphorylation levels may be due to different VEGF dosage and VEGFR2 density in the cells used for these experiments (Tan et al., 2013). VEGFR2 density can vary between different EC types (Tan et al., 2013), suggesting that the use of different cell types (HUVECs and TIME cells) might alter VEGFR2 trafficking in response to VEGFA and thereby impact the magnitude and duration of Erk phosphorylation. In addition, the decrease in Erk 1/2 phosphorylation could also be due to blocking or reducing the intracellular trafficking of VEGFR2, thereby suppressing VEGFA-induced Erk 1/2 phosphorylation (Lanahan et al., 2010). We also do not exclude, since there is a trend for decreased Erk 1/2 phosphorylation in *PTPRB*-depleted cells at basal conditions, that negative feedback loops that target components of the Erk 1/2 pathway may be activated, thereby suppressing signalling downstream of the receptor (Lake et al., 2016; Pontes-Quero et al.,

2019). Moreover, our results are supported by three replicated independent experiments at different times of VEGFA stimulation, while in Mellberg et al., a single experiment comparing basal conditions and 5 minutes VEGFA (20 ng/ml) stimulation is shown. This suggests that in stimulated HUVECs, *PTPRB* silencing may affect VEGFR2 trafficking resulting in reduced Erk 1/2 phosphorylation. Furthermore, VEGFR2 Y1175 phosphorylation is known to activate Erk 1/2 signalling through phospholipase Cγ (PLCγ) or protein kinase C (PKC) (Simons et al., 2016). Therefore, we do not exclude that decreased Erk 1/2 signalling in *PTPRB*-deficient cells may depend on altered PKC or PLCγ activation in response to VEGFA.

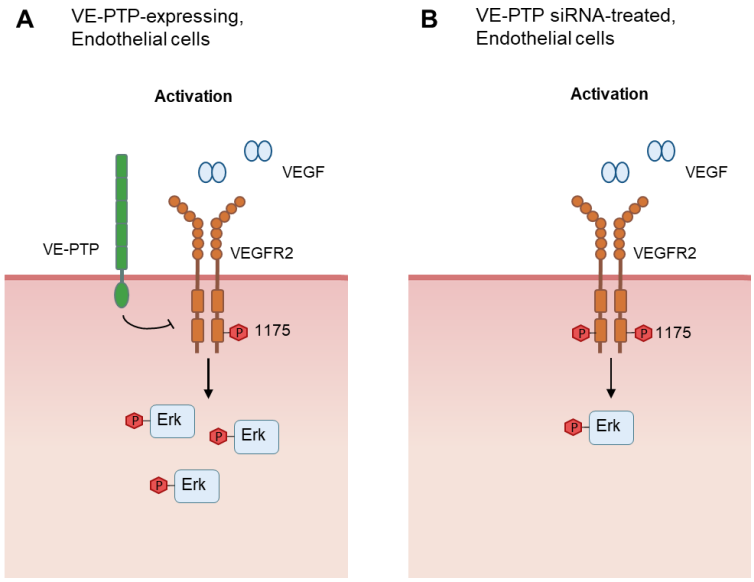

Figure 4.1. Schematic of the consequence of reduced *PTPRB* expression on VEGFA stimulated cells. (A) VEGFA stimulation of ECs expressing *PTPRB* induces phosphorylation (p) of VEGFR2 at site Y1175 and activation of the downstream signal transducer Erk 1/2. **(B)** VEGFA stimulation in ECs after *PTPRB* siRNA transfection, further enhances phosphorylation of VEGFR2 at Y1175, but decreases Erk 1/2 phosphorylation.

Increased tyrosine phosphorylation of VEGFR2 and activation of downstream signalling pathways in response to *PTPRB* silencing has been shown to affect the VEGFA-response during angiogenesis (Hayashi et al., 2013). In addition, VE-PTP inactivation and subsequent enhanced tyrosine phosphorylation of VEGFR2 and VE-cadherin resulted in loss of cell polarity and lumen formation in mouse embryoid bodies (Hayashi et al., 2013). In this study, we showed that *Ptprb* iECKO impaired retina vascular development, reducing vessel density, vessel outgrowth from the optic nerve and tip cell density (Figure 3.8C). Interestingly, VE-PTP inhibition with a single dose of intraocular injection of AKB-9778 at P4, has previously been shown to have no effect on vascularization of the retina surface at P7 (Shen et al., 2014), suggesting that repeated doses or higher concentrations are necessary for efficient VE-PTP inhibition. Moreover, our findings of increased VEGFR2 Y1175 phosphorylation to above normal levels, in *PTPRB*-depleted cells (Figure 3.5), together with the established role of VE-PTP in dephosphorylating VEGFR2 in stalk cells (Hayashi et al., 2013), suggest that VE-PTP ablation in ECs during angiogenesis may interfere with EC proliferation by increasing stalk cell responsiveness to VEGFA.

We also found that *PTPRB* silencing decreased VEGFA-induced Erk 1/2 signalling in cells (Figure 3.6). VEGFR2 Y1175 downstream induction of Erk 1/2 is known to regulate cell

proliferation (Simons et al., 2016) and a reduction in Erk 1/2 signalling *in vivo* in *PTPRB*-depleted ECs could explain the observed reduction in retina vessel outgrowth and vessel density. However, to confirm this model, phosphorylated Erk 1/2 and total Erk 1/2 levels should be determined in the developing retina, which was not yet carried out in this study.

Although, Tie2 signalling was not explored in this study, VE-PTP is known to have a role in determining the context-dependent function of the Tie2 ligand ANGPT2 (Souma et al., 2018) as well as in inactivating ANGPT1/Tie2 signalling pathway (Fachinger et al., 1999; Goel et al., 2013). Furthermore, ANGPT2 is required for postnatal vascular remodelling in the eye, playing a distinct function of ANGPT1 (Gale et al., 2002). We speculate that lack of VE-PTP might induce environmental changes in the mouse retina, which change ANGPT2 agonistic function, compromising normal development of the vasculature. This hypothesis is supported by the abnormal outgrowth of retinal capillaries in mice homozygous for A*ngpt*2 deletion (Gale et al., 2002). Moreover, ANGPT2 is also thought to promote retinal vessel sensitivity to VEGF (Oshima et al., 2004), which is highly expressed in the initially avascular retina (Stone et al., 1995). Additionally, we did not find any difference in the expression levels of *Tie2*, *Flk1* and *Cdh5* upon *Ptprb* gene deletion in ECs (Figure 3.9). This shows that VE-PTP´s regulation of retina vascular development occurs by a mechanism that is independent of VEGFR2, Tie2 and VE-cadherin expression levels.

In the OIR, an angiogenesis model for ischemic retinopathy, exposure of mice to hyperoxia from P7 to P12, induces obliteration of the capillaries in the centre of the retina by suppressed VEGFA expression. This is followed by returning pups to room air where the retina experiences a relative hypoxia, resulting in enhanced VEGFA expression, triggering NV and the formation of NV tufts from P12 to P17 (Dai et al., 2021; Scott & Fruttiger, 2009). Since *PTPRB* silencing was shown to promote VEGFA-induced phosphorylation of VEGFR2 at Y1175 (Figure 3.5), we studied the impact of *Ptprb* deletion during abnormal angiogenesis. We observed that the retina avascular area was decreased in P17 *Ptprb* iECKO retinas (Figure 3.10C). Even though, VEGFA expression is reduced in hyperoxia conditions, this suggests that increased VEGFA-induced VEGFR2 phosphorylation in the absence of VE-PTP could slightly compensate for low levels of VEGFA which are associated with suppressed blood vessel growth (Penn et al., 2008). Thus, deletion of *Ptprb* during hyperoxia may increase VEGFR2 sensitivity to low levels of VEGFA, resulting in reduced vascular obliteration.

In diabetes and ischemic retinopathy, hypoxia in vascular endothelial cell, as in retinal NV, upregulates VE-PTP expression, thereby reducing Tie2 activity (Carota et al., 2019; Shen et al., 2014). Therefore, we hypothesised that *Ptprb* ablation during hypoxic conditions would reduce retinal NV through activation of the ANGPT1/Tie2 pathway. Surprisingly, no significant difference was observed in the tuft number or area of *Ptprb* iECKO mice compare to control littermates. However, in laser-induced choroidal NV mouse model to study age-related macular degeneration, inhibition of VEPTP´s catalytic activity with AKB-9778 supressed subretinal NV (Shen et al., 2014). AKB-9778 appeared to selectively accentuate ANGPT2 agonistic function during NV (Shen et al., 2014), a process that is stimulated by high levels of ANGPT2 and VEGF (Eklund & Olsen, 2006). This indicates that VE-PTP may have different roles depending on the retinopathy model in study, since inhibition of VE-PTP had different

outcomes depending on the disease model used. Nonetheless, it needs to be taken into account that the experiments conducted in this study should be repeated due to the low number of control mice (*Ptprb*$^{fl/fl}$) used for statistical analyses. Overall, these studies reinforce the need for more accurate models that better mimic human ischemic retinopathies, in order to allow the study of a specific pathway inhibition in disease outcome in a more reliable way.

Although, there was no significant difference in the tuft area or tuft number (Figure 3.10D-E), we observed a difference in tuft morphology between *Ptprb*$^{fl/fl}$*;Cdh5-CreERT2* and *Ptprb*$^{fl/fl}$ mice. Neovascular tufts were smaller in tamoxifen-induced *Ptprb*$^{fl/fl}$*;Cdh5-CreERT2* mice compared to *Ptprb*$^{fl/fl}$ littermates that showed more disperse and dilated tufts (Figure 5.2, in appendix). The tendency for an increased number of tufts (Figure 3.10E) in *Ptptb*-depleted mice might explain the similar tuft area between *Ptprb*$^{fl/fl}$*;Cdh5-CreERT2* and *Ptprb*$^{fl/fl}$ mice (Figure 3.10D). However, flat-mounting retinas for confocal imaging distorts tissue morphology, and thereby it is not a reliable technique to observe tuft morphology. Instead 3D imaging of the retinas with light-sheet fluorescence microscopy, which allows better analyses of neovascular structures, should be used since it provides a better understanding of tuft morphology than possible with 2D analyses (Prahst et al., 2020).

5. Conclusion

The present study revealed that VE-PTP has an important role *in vitro* in regulating VEGFR2 signalling and its downstream signalling transducer Erk 1/2. Moreover, VE-PTP function during development of the mouse retinal vasculature and in a mouse model of pathologic angiogenesis was determined using an inducible endothelial specific *Ptprb* knockout mouse line.

In this work all *in vitro* studies were performed on HUVECs. First, *PTPRB* siRNA efficiency was determined by RT-qPCR with RNA isolated from cells transfected for 48 hours with a range of siRNA concentrations. Silencing of human *PTPRB* was efficiently obtained after transfection with 20 nM of *PTPRB* siRNA, as observed in RT-qPCR for human *PTPRB*. Immunoblotting of transfected cells with commercially available VE-PTP antibodies, including one customer-generated VE-PTP antibody, further confirmed the transfection efficiency of the *PTPRB* siRNA and the specificity of HPA002700, HPA054453 and Storkbio antibodies, but not Biorbyt and Invitrogen antibodies, for the human VE-PTP protein. *PTPRB* silencing increased VEGFA-induced phosphorylation of VEGFR2 at Y1175 compared to control. However, in the same conditions a decrease in Erk 1/2 phosphorylation was observed. Immunostaining for VE-PTP and VE-cadherin showed that VE-PTP colocalizes with VE-cadherin at EC junctions, allowing VE-PTP to interact with VEGFR2.

The impact of *Ptprb* deletion was explored *in vivo* using a tamoxifen inducible EC *Ptprb* knockout mouse line. *Ptprb* floxing efficiency was determined using lung tissue of P6 *Ptprb*$^{fl/fl}$*;Cdh5-CreERT2* and *Ptprb*$^{fl/fl}$ mice treated with tamoxifen. RT-qPCR for mouse *Ptprb* and VE-PTP immunoblots, confirmed efficient Cre activation and deletion of floxed *Ptprb* alleles in *Ptprb*$^{fl/fl}$*;Cdh5-CreERT2* mice following tamoxifen injection. Postnatal *Ptprb* gene ablation in P6 mice resulted in impaired retina vascular development, determined by reduced vessel density, vessel outgrowth and tip cell density. These phenotypic alterations were not associated with changes in the expression levels of *Tie2*, *Flk1* and *Cdh5*. In the OIR mouse model of ischemia-induced angiogenesis in the retinal vasculature, *Ptprb* iECKO at P17 reduced retina avascular area. However, deletion of *Ptprb* had no effect on neovascular tuft number or area.

The current findings indicate that VE-PTP is required *in vivo* for the normal development of the retinal vasculature. We hypothesize that impaired vascular development in *Ptprb*

iECKO might be due to decreased Erk 1/2 phosphorylation in response to VEGFA, as observed *in vitro*. However, more experiments are required to confirm this mechanism *in vivo*. In an ischemic disease mouse model, oxygen-induced retinopathy, *Ptprb* deletion reduced vessel obliteration possible by increasing VEGFR2 sensitivity to VEGFA, as shown in *in vitro* assays. Although, there were no differences on NV tufts in these mice, a trend for increased tuft number and changes in tuft morphology between *Ptprb*$^{fl/fl}$*;Cdh5-CreERT2* and *Ptprb*$^{fl/fl}$ mice were observed. Nevertheless, tuft morphology should be assessed with more reliable imaging methods, such as 3D light-sheet fluorescence microscopy, since 2D retina analyses distorts tissue morphology. Most importantly, retina analyses should be repeated due to the low number of *Ptprb*$^{fl/fl}$ mice used for statistical analyses.

In conclusion, our data supports VE-PTP as a potential target to counteract VEGFA-induced VEGFR2 activity, responsible for the onset of several pathologies, including ischemic proliferative diseases. However, the reduced pErk 1/2 induction in response to VEGFA in *PTPRB*-deficient ECs complicates conclusions. Thus, more studies are warranted.

BIBLIOGRAPHY

Abhinand, C. S., Raju, R., Soumya, S. J., Arya, P. S., & Sudhakaran, P. R. (2016). VEGF-A/VEGFR2 signaling network in endothelial cells relevant to angiogenesis. *Journal of Cell Communication and Signaling*, *10*(4), 347–354. https://doi.org/10.1007/S12079-016-0352-8

Akwii, R. G., & Mikelis, C. M. (2021). Targeting the Angiopoietin/Tie Pathway: Prospects for Treatment of Retinal and Respiratory Disorders. *Drugs*, 1–19. https://doi.org/10.1007/S40265-021-01605-Y

Alberts, B., Johnson, A., Lewis, J., Raff, M., Roberts, K., & Walter, P. (2002). Blood Vessels and Endothelial Cells. In *Molecular Biology of the Cell* (4th ed.). New York: Garland Science. https://www.ncbi.nlm.nih.gov/books/NBK26848/

Arif, N., Zinnhardt, M., Nyamay'Antu, A., Teber, D., Brückner, R., Schaefer, K., Li, Y.-T., Trappmann, B., Grashoff, C., & Vestweber, D. (2021). PECAM-1 supports leukocyte diapedesis by tension-dependent dephosphorylation of VE-cadherin. *The EMBO Journal*, *40*(9), e106113. https://doi.org/10.15252/EMBJ.2020106113

Azzi, S., Hebda, J. K., & GAVARD, J. (2013). Vascular Permeability and Drug Delivery in Cancers. *Frontiers in Oncology*, *3*, 211. https://doi.org/10.3389/FONC.2013.00211

Bäumer, S., Keller, L., Holtmann, A., Funke, R., August, B., Gamp, A., Wolburg, H., Wolburg-Buchholz, K., Deutsch, U., & Vestweber, D. (2006). Vascular endothelial cell-specific phosphotyrosine phosphatase (VE-PTP) activity is required for blood vessel development. *Blood*, *107*(12), 4754–4762. https://doi.org/10.1182/blood-2006-01-0141

Bilimoria, J., & Singh, H. (2019). The Angiopoietin ligands and Tie receptors: potential diagnostic biomarkers of vascular disease. *Journal of Receptors and Signal Transduction*, *39*(3), 187–193. https://doi.org/10.1080/10799893.2019.1652650

Brash, J. T., Bolton, R. L., Rashbrook, V. S., Denti, L., Kubota, Y., & Ruhrberg, C. (2020). Tamoxifen-Activated CreERT Impairs Retinal Angiogenesis Independently of Gene Deletion. *Circulation Research*, *127*(6), 849–850. https://doi.org/10.1161/CIRCRESAHA.120.317025

Braun, L. J., Stegmeyer, R. I., Schäfer, K., Volkery, S., Currie, S. M., Kempe, B., Nottebaum, A. F., & Vestweber, D. (2020). Platelets docking to VWF prevent leaks during leukocyte extravasation by stimulating Tie-2. *Blood*, *136*(5), 627–639. https://doi.org/10.1182/BLOOD.2019003442

Braun, L. J., Zinnhardt, M., Vockel, M., Drexler, H. C., Peters, K., & Vestweber, D. (2019). VE-PTP inhibition stabilizes endothelial junctions by activating FGD5. *EMBO Reports*, *20*(7), e47046. https://doi.org/10.15252/EMBR.201847046

Broermann, A., Winderlich, M., Block, H., Frye, M., Rossaint, J., Zarbock, A., Cagna, G., Linnepe, R., Schulte, D., Nottebaum, A. F., & Vestweber, D. (2011). Dissociation of VE-PTP from VE-cadherin is required for leukocyte extravasation and for VEGF-induced vascular permeability in vivo. *The Journal of Experimental Medicine*, *208*(12), 2393–2401.

https://doi.org/10.1084/JEM.20110525
Campochiaro, P. A., Khanani, A., Singer, M., Patel, S., Boyer, D., Dugel, P., Kherani, S., Withers, B., Gambino, L., Peters, K., & Brigell, M. (2016). Enhanced Benefit in Diabetic Macular Edema from AKB-9778 Tie2 Activation Combined with Vascular Endothelial Growth Factor Suppression. *Ophthalmology*, *123*(8), 1722–1730. https://doi.org/10.1016/J.OPHTHA.2016.04.025
Carmeliet, P., Ferreira, V., Breier, G., Pollefeyt, S., Kieckens, L., Gertsenstein, M., Fahrig, M., Vandenhoeck, A., Harpal, K., Eberhardt, C., Declercq, C., Pawling, J., Moons, L., Collen, D., Risau, W., & Nagy, A. (1996). Abnormal blood vessel development and lethality in embryos lacking a single VEGF allele. *Nature*, *380*(6573), 435–439. https://doi.org/10.1038/380435a0
Carmeliet, P., & Jain, R. K. (2011). Molecular mechanisms and clinical applications of angiogenesis. *Nature*, *473*(7347), 298–307. https://doi.org/10.1038/NATURE10144
Carmeliet, P., Lampugnani, M.-G., Moons, L., Breviario, F., Compernolle, V., Bono, F., Balconi, G., Spagnuolo, R., Oosthuyse, B., Dewerchin, M., Zanetti, A., Angellilo, A., Mattot, V., Nuyens, D., Lutgens, E., Clotman, F., Ruiter, M. C. de, Groot, A. G., Poelmann, R., … Dejana, E. (1999). Targeted Deficiency or Cytosolic Truncation of the VE-cadherin Gene in Mice Impairs VEGF-Mediated Endothelial Survival and Angiogenesis. *Cell*, *98*(2), 147–157. https://doi.org/10.1016/S0092-8674(00)81010-7
Carota, I. A., Kenig-Kozlovsky, Y., Onay, T., Scott, R., Thomson, B. R., Souma, T., Bartlett, C. S., Li, Y., Procissi, D., Ramirez, V., Yamaguchi, S., Tarjus, A., Tanna, C. E., Li, C., Eremina, V., Vestweber, D., Oladipupo, S. S., Breyer, M. D., & Quaggin, S. E. (2019). Targeting VE-PTP phosphatase protects the kidney from diabetic injury. *Journal of Experimental Medicine*, *216*(4), 936–949. https://doi.org/10.1084/jem.20180009
Cheng, C., Haasdijk, R., Tempel, D., Kamp, E. H. M. van de, Herpers, R., Bos, F., Dekker, W. K. Den, Blonden, L. A. J., Jong, R. de, Bürgisser, P. E., Chrifi, I., Biessen, E. A. L., Dimmeler, S., Schulte-Merker, S., & Duckers, H. J. (2012). Endothelial Cell–Specific FGD5 Involvement in Vascular Pruning Defines Neovessel Fate in Mice. *Circulation*, *125*(25), 3142–3159. https://doi.org/10.1161/CIRCULATIONAHA.111.064030
Claesson-Welsh, L. (2015). Vascular permeability—the essentials. *Upsala Journal of Medical Sciences*, *120*(3), 135. https://doi.org/10.3109/03009734.2015.1064501
Claesson-Welsh, L., Dejana, E., & McDonald, D. M. (2021). Permeability of the Endothelial Barrier: Identifying and Reconciling Controversies. *Trends in Molecular Medicine*, *27*(4), 314–331. https://doi.org/10.1016/J.MOLMED.2020.11.006
Cochrane, A., Albers, H. J., Passier, R., Mummery, C. L., van den Berg, A., Orlova, V. V., & van der Meer, A. D. (2019). Advanced in vitro models of vascular biology: Human induced pluripotent stem cells and organ-on-chip technology. *Advanced Drug Delivery Reviews*, *140*, 68–77. https://doi.org/10.1016/J.ADDR.2018.06.007
Connor, K. M., Krah, N. M., Dennison, R. J., Aderman, C. M., Chen, J., Guerin, K. I., Sapieha, P., Stahl, A., Willett, K. L., & Smith, L. E. H. (2009). Quantification of oxygen-induced retinopathy in the mouse: a model of vessel loss, vessel regrowth and pathological angiogenesis. *Nature Protocols 2009 4:11*, *4*(11), 1565–1573. https://doi.org/10.1038/nprot.2009.187
Corti, F., & Simons, M. (2017). Modulation of VEGF receptor 2 signaling by protein phosphatases. *Pharmacological Research*, *115*, 107–123. https://doi.org/10.1016/j.phrs.2016.11.022
Coultas, L., Chawengsaksophak, K., & Rossant, J. (2005). Endothelial cells and VEGF in vascular development. *Nature*, *438*, 937–945. https://doi.org/10.1038/nature04479
Dai, C., Webster, K. A., Bhatt, A., Tian, H., Su, G., & Li, W. (2021). Concurrent Physiological and Pathological Angiogenesis in Retinopathy of Prematurity and Emerging Therapies. *International Journal of Molecular Sciences*, *22*(9), 4809.

https://doi.org/10.3390/IJMS22094809
Delgado-Bellido, D., Bueno-Galera, C., López-Jiménez, L., Garcia-Diaz, A., & Oliver, F. J. (2020). Endothelial Phosphatase VE-PTP Participates in Vasculogenic Mimicry by Preventing Autophagic Degradation of VE-Cadherin. *Frontiers in Oncology*, *10*, 18. https://doi.org/10.3389/FONC.2020.00018
Dominguez, M. G., Hughes, V. C., Pan, L., Simmons, M., Daly, C., Anderson, K., Noguera-Troise, I., Murphy, A. J., Valenzuela, D. M., Davis, S., Thurston, G., Yancopoulos, G. D., & Gale, N. W. (2007). Vascular endothelial tyrosine phosphatase (VE-PTP)-null mice undergo vasculogenesis but die embryonically because of defects in angiogenesis. *Proceedings of the National Academy of Sciences*, *104*(9), 3243–3248. https://doi.org/10.1073/PNAS.0611510104
Dong, D., & Yang, P. (2018). Yolk Sac. In *Encyclopedia of Reproduction* (2nd ed., Vol. 2, pp. 551–558). Academic Press. https://doi.org/10.1016/B978-0-12-801238-3.64685-8
Drexler, H. C. A., Vockel, M., Polaschegg, C., Frye, M., Peters, K., & Vestweber, D. (2019). Vascular Endothelial Receptor Tyrosine Phosphatase: Identification of Novel Substrates Related to Junctions and a Ternary Complex with EPHB4 and TIE2. *Molecular and Cellular Proteomics*, *18*(10), 2058–2077. https://doi.org/10.1074/MCP.RA119.001716
Du, E., Li, X., He, S., Li, X., & He, S. (2020). The critical role of the interplays of EphrinB2/EphB4 and VEGF in the induction of angiogenesis. *Molecular Biology Reports*, *47*(6), 4681–4690. https://doi.org/10.1007/S11033-020-05470-Y
Eitzen, G., Smithers, C. C., Murray, A. G., & Overduin, M. (2018). Structure and function of the Fgd family of divergent FYVE domain proteins. *Biochemistry and Cell Biology*, *97*(3), 257–264. https://doi.org/10.1139/BCB-2018-0185
Eklund, L., & Olsen, B. R. (2006). Tie receptors and their angiopoietin ligands are context-dependent regulators of vascular remodeling. *Experimental Cell Research*, *312*(5), 630–641. https://doi.org/10.1016/J.YEXCR.2005.09.002
Erber, R., Eichelsbacher, U., Powajbo, V., Korn, T., Djonov, V., Lin, J., Hammes, H.-P., Grobholz, R., Ullrich, A., & Vajkoczy, P. (2006). EphB4 controls blood vascular morphogenesis during postnatal angiogenesis. *The EMBO Journal*, *25*(3), 628–641. https://doi.org/10.1038/SJ.EMBOJ.7600949
Fachinger, G., Deutsch, U., & Risau, W. (1999). Functional interaction of vascular endothelial-protein-tyrosine phosphatase with the angiopoietin receptor Tie-2. *Oncogene*, *18*(43), 5948–5953. https://doi.org/10.1038/SJ.ONC.1202992
Fantin, A., Vieira, J. M., Gestri, G., Denti, L., Schwarz, Q., Prykhozhij, S., Peri, F., Wilson, S. W., & Ruhrberg, C. (2010). Tissue macrophages act as cellular chaperones for vascular anastomosis downstream of VEGF-mediated endothelial tip cell induction. *Blood*, *116*(5), 829–840. https://doi.org/10.1182/BLOOD-2009-12-257832
Ferrara, N., & Adamis, A. P. (2016). Ten years of anti-vascular endothelial growth factor therapy. *Nature Reviews Drug Discovery*, *15*(6), 385–403. https://doi.org/10.1038/nrd.2015.17
Ferrara, N., Carver-Moore, K., Chen, H., Dowd, M., Lu, L., O'Shea, K. S., Powell-Braxton, L., Hillan, K. J., & Moore, M. W. (1996). Heterozygous embryonic lethality induced by targeted inactivation of the VEGF gene. *Nature*, *380*(6573), 439–442. https://doi.org/10.1038/380439a0
Frye, M., Dierkes, M., Küppers, V., Vockel, M., Tomm, J., Zeuschner, D., Rossaint, J., Zarbock, A., Koh, G. Y., Peters, K., Nottebaum, A. F., & Vestweber, D. (2015). Interfering with VE-PTP stabilizes endothelial junctions in vivo via Tie-2 in the absence of VE-cadherin. *The Journal of Experimental Medicine*, *212*(13), 2267–2287. https://doi.org/10.1084/JEM.20150718
Gale, N. W., Thurston, G., Hackett, S. F., Renard, R., Wang, Q., McClain, J., Martin, C., Witte, C., Witte, M. H., Jackson, D., Suri, C., Campochiaro, P. A., Wiegand, S. J., & Yancopoulos,

G. D. (2002). Angiopoietin-2 Is Required for Postnatal Angiogenesis and Lymphatic Patterning, and Only the Latter Role Is Rescued by Angiopoietin-1. *Developmental Cell*, *3*(3), 411–423. https://doi.org/10.1016/S1534-5807(02)00217-4

Gerety, S. S., Wang, H. U., Chen, Z.-F., & Anderson, D. J. (1999). Symmetrical Mutant Phenotypes of the Receptor EphB4 and Its Specific Transmembrane Ligand ephrin-B2 in Cardiovascular Development. *Molecular Cell*, *4*(3), 403–414. https://doi.org/10.1016/S1097-2765(00)80342-1

Gerhardt, H., Golding, M., Fruttiger, M., Ruhrberg, C., Lundkvist, A., Abramsson, A., Jeltsch, M., Mitchell, C., Alitalo, K., Shima, D., & Betsholtz, C. (2003). VEGF guides angiogenic sprouting utilizing endothelial tip cell filopodia. *Journal of Cell Biology*, *161*(6), 1163–1177. https://doi.org/10.1083/JCB.200302047

Giannotta, M., Trani, M., & Dejana, E. (2013). VE-cadherin and endothelial adherens junctions: Active guardians of vascular integrity. *Developmental Cell*, *26*(5), 441–454. https://doi.org/10.1016/j.devcel.2013.08.020

Goel, S., Gupta, N., Walcott, B. P., Snuderl, M., Kesler, C. T., Kirkpatrick, N. D., Heishi, T., Huang, Y., Martin, J. D., Ager, E., Samuel, R., Wang, S., Yazbek, J., Vakoc, B. J., Peterson, R. T., Padera, T. P., Duda, D. G., Fukumura, D., & Jain, R. K. (2013). Effects of vascular-endothelial protein tyrosine phosphatase inhibition on breast cancer vasculature and metastatic progression. *Journal of the National Cancer Institute*, *105*(16), 1188–1201. https://doi.org/10.1093/jnci/djt164

Gong, H., Rehman, J., Tang, H., Wary, K., Mittal, M., Chatturvedi, P., Zhao, Y., Komorova, Y. A., Vogel, S. M., & Malik, A. B. (2015). HIF2α signaling inhibits adherens junctional disruption in acute lung injury. *The Journal of Clinical Investigation*, *125*(2), 652–664. https://doi.org/10.1172/JCI77701

Guo, Y., Pan, W., Liu, S., Shen, Z., Xu, Y., & Hu, L. (2020). ERK/MAPK signalling pathway and tumorigenesis (Review). *Experimental and Therapeutic Medicine*, *19*(3), 1997–2007. https://doi.org/10.3892/ETM.2020.8454

Gurnik, S., Devraj, K., Macas, J., Yamaji, M., Starke, J., Scholz, A., Sommer, K., Tacchio, M. Di, Vutukuri, R., Beck, H., Mittelbronn, M., Foerch, C., Pfeilschifter, W., Liebner, S., Peters, K. G., Plate, K. H., & Reiss, Y. (2016). Angiopoietin-2-induced blood–brain barrier compromise and increased stroke size are rescued by VE-PTP-dependent restoration of Tie2 signaling. *Acta Neuropathologica*, *131*(5), 753–773. https://doi.org/10.1007/S00401-016-1551-3

Hayashi, M., Majumdar, A., Li, X., Adler, J., Sun, Z., Vertuani, S., Hellberg, C., Mellberg, S., Koch, S., Dimberg, A., Young Koh, G., Dejana, E., Belting, H. G., Affolter, M., Thurston, G., Holmgren, L., Vestweber, D., & Claesson-Welsh, L. (2013). VE-PTP regulates VEGFR2 activity in stalk cells to establish endothelial cell polarity and lumen formation. *Nature Communications*, *4*, 1615–1672. https://doi.org/10.1038/ncomms2683

Jain, R. K. (2003). Molecular regulation of vessel maturation. *Nature Medicine*, *9*, 685–693. https://doi.org/10.1038/nm0603-685

Juettner, V. V., Kruse, K., Dan, A., Vu, V. H., Khan, Y., Le, J., Leckband, D., Komarova, Y., & Malik, A. B. (2019). VE-PTP stabilizes VE-cadherin junctions and the endothelial barrier via a phosphatase-independent mechanism. *Journal of Cell Biology*, *218*(5), 1725–1742. https://doi.org/10.1083/jcb.201807210

Kim, C. B., D'Amore, P. A., & Connor, K. M. (2016). Revisiting the mouse model of oxygen-induced retinopathy. *Eye and Brain*, *8*, 67–79. https://doi.org/10.2147/EB.S94447

Kim, H., Kim, M., Im, S.-K., & Fang, S. (2018). Mouse Cre-LoxP system: general principles to determine tissue-specific roles of target genes. *Laboratory Animal Research*, *34*(4), 147–159. https://doi.org/10.5625/LAR.2018.34.4.147

Kim, M., Allen, B., Korhonen, E. A., Nitschké, M., Yang, H. W., Baluk, P., Saharinen, P., Alitalo, K., Daly, C., Thurston, G., & McDonald, D. M. (2016). Opposing actions of angiopoietin-

2 on Tie2 signaling and FOXO1 activation. *The Journal of Clinical Investigation*, *126*(9), 3511–3525. https://doi.org/10.1172/JCI84871

Kocherova, I., Bryja, A., Mozdziak, P., Volponi, A. A., Dyszkiewicz-Konwińska, M., Piotrowska-Kempisty, H., Antosik, P., Bukowska, D., Bruska, M., Iżycki, D., Zabel, M., Nowicki, M., & Kempisty, B. (2019). Human Umbilical Vein Endothelial Cells (HUVECs) Co-Culture with Osteogenic Cells: From Molecular Communication to Engineering Prevascularised Bone Grafts. *Journal of Clinical Medicine*, *8*(10), 1602. https://doi.org/10.3390/JCM8101602

Korhonen, E. A., Lampinen, A., Giri, H., Anisimov, A., Kim, M., Allen, B., Fang, S., D'Amico, G., Sipilä, T. J., Lohela, M., Strandin, T., Vaheri, A., Ylä-Herttuala, S., Koh, G. Y., McDonald, D. M., Alitalo, K., & Saharinen, P. (2016). Tie1 controls angiopoietin function in vascular remodeling and inflammation. *The Journal of Clinical Investigation*, *126*(9), 3495–3510. https://doi.org/10.1172/JCI84923

Krüger-Genge, A., Blocki, A., Franke, R. P., & Jung, F. (2019). Vascular endothelial cell biology: An update. *International Journal of Molecular Sciences*, *20*(18). https://doi.org/10.3390/ijms20184411

Lake, D., Corrêa, S. A. L., & Müller, J. (2016). Negative feedback regulation of the ERK1/2 MAPK pathway. *Cellular and Molecular Life Sciences*, *73*(23), 4397–4413. https://doi.org/10.1007/S00018-016-2297-8

Lampreht Tratar, U., Horvat, S., & Cemazar, M. (2018). Transgenic Mouse Models in Cancer Research. *Frontiers in Oncology*, *8*, 268. https://doi.org/10.3389/FONC.2018.00268

Lanahan, A. A., Hermans, K., Claes, F., Kerley-Hamilton, J. S., Zhuang, Z. W., Giordano, F. J., Carmeliet, P., & Simons, M. (2010). VEGF receptor 2 endocytic trafficking regulates arterial morphogenesis. *Developmental Cell*, *18*(5), 713–724. https://doi.org/10.1016/J.DEVCEL.2010.02.016

Li, G., Nottebaum, A. F., Brigell, M., Navarro, I. D., Ipe, U., Mishra, S., Gomez-Caraballo, M., Schmitt, H., Soldo, B., Pakola, S., Withers, B., Peters, K. G., Vestweber, D., & Stamer, W. D. (2020). A Small Molecule Inhibitor of VE-PTP Activates Tie2 in Schlemm's Canal Increasing Outflow Facility and Reducing Intraocular Pressure. *Investigative Ophthalmology & Visual Science*, *61*(14). https://doi.org/10.1167/IOVS.61.14.12

Li, X., Padhan, N., Sjöström, E. O., Roche, F. P., Testini, C., Honkura, N., Sáinz-Jaspeado, M., Gordon, E., Bentley, K., Philippides, A., Tolmachev, V., Dejana, E., Stan, R. V., Vestweber, D., Ballmer-Hofer, K., Betsholtz, C., Pietras, K., Jansson, L., & Claesson-Welsh, L. (2016). VEGFR2 pY949 signalling regulates adherens junction integrity and metastatic spread. *Nature Communications*, *7*. https://doi.org/10.1038/ncomms11017

Li, Z., Huang, H., Boland, P., Dominguez, M. G., Burfeind, P., Lai, K.-M., Lin, H.-C., Gale, N. W., Daly, C., Auerbach, W., Valenzuela, D., Yancopoulos, G. D., & Thurston, G. (2009). Embryonic stem cell tumor model reveals role of vascular endothelial receptor tyrosine phosphatase in regulating Tie2 pathway in tumor angiogenesis. *Proceedings of the National Academy of Sciences*, *106*(52), 22399–22404. https://doi.org/10.1073/PNAS.0911189106

Markiewski, M. M., Daugherity, E., Reese, B., & Karbowniczek, M. (2020). The Role of Complement in Angiogenesis. *Antibodies (Basel, Switzerland)*, *9*(4), 67. https://doi.org/10.3390/ANTIB9040067

Matsumoto, T., Bohman, S., Dixelius, J., Berge, T., Dimberg, A., Magnusson, P., Wang, L., Wikner, C., Qi, J. H., Wernstedt, C., Wu, J., Bruheim, S., Mugishima, H., Mukhopadhyay, D., Spurkland, A., & Claesson-Welsh, L. (2005). VEGF receptor-2 Y951 signaling and a role for the adapter molecule TSAd in tumor angiogenesis. *The EMBO Journal*, *24*(13), 2342–2353. https://doi.org/10.1038/SJ.EMBOJ.7600709

McLellan, M. A., Rosenthal, N. A., & Pinto, A. R. (2017). Cre-loxP-Mediated Recombination: General Principles and Experimental Considerations. *Current Protocols in Mouse Biology*, *7*(1), 1–12. https://doi.org/10.1002/CPMO.22

Mellberg, S., Dimberg, A., Bahram, F., Hayashi, M., Rennel, E., Ameur, A., Westholm, J. O., Larsson, E., Lindahl, P., Cross, M. J., & Claesson-Welsh, L. (2009). Transcriptional profiling reveals a critical role for tyrosine phosphatase VE-PTP in regulation of VEGFR2 activity and endothelial cell morphogenesis. *The FASEB Journal*, *23*(5), 1490–1502. https://doi.org/10.1096/fj.08-123810

Montero-Balaguer, M., Swirsding, K., Orsenigo, F., Cotelli, F., Mione, M., & Dejana, E. (2009). Stable Vascular Connections and Remodeling Require Full Expression of VE-Cadherin in Zebrafish Embryos. *PLoS One*, *4*(6), e5772. https://doi.org/10.1371/JOURNAL.PONE.0005772

Mori, M., Murata, Y., Kotani, T., Kusakari, S., Ohnishi, H., Saito, Y., Okazawa, H., Ishizuka, T., Mori, M., & Matozaki, T. (2010). Promotion of cell spreading and migration by Vascular Endothelial-Protein Tyrosine Phosphatase (VE-PTP) in cooperation with integrins. *Journal of Cellular Physiology*, *224*(1), 195–204. https://doi.org/10.1002/jcp.22122

Nawroth, R., Poell, G., Ranft, A., Kloep, S., Samulowitz, U., Fachinger, G., Golding, M., Shima, D. T., Deutsch, U., & Vestweber, D. (2002). VE-PTP and VE-cadherin ectodomains interact to facilitate regulation of phosphorylation and cell contacts. *EMBO Journal*, *21*(18), 4885–4895. https://doi.org/10.1093/EMBOJ/CDF497

Nottebaum, A. F., Cagna, G., Winderlich, M., Gamp, A. C., Linnepe, R., Polaschegg, C., Filippova, K., Lyck, R., Engelhardt, B., Kamenyeva, O., Bixel, M. G., Butz, S., & Vestweber, D. (2008). VE-PTP maintains the endothelial barrier via plakoglobin and becomes dissociated from VE-cadherin by leukocytes and by VEGF. *Journal of Experimental Medicine*, *205*(12), 2929–2945. https://doi.org/10.1084/JEM.20080406

Olsson, A.-K., Dimberg, A., Kreuger, J., & Claesson-Welsh, L. (2006). VEGF receptor signalling - in control of vascular function. *Nature Reviews Molecular Cell Biology*, *7*(5), 359–371. https://doi.org/10.1038/NRM1911

Orsenigo, F., Giampietro, C., Ferrari, A., Corada, M., Galaup, A., Sigismund, S., Ristagno, G., Maddaluno, L., Young Koh, G., Franco, D., Kurtcuoglu, V., Poulikakos, D., Baluk, P., McDonald, D., Grazia Lampugnani, M., & Dejana, E. (2012). Phosphorylation of VE-cadherin is modulated by haemodynamic forces and contributes to the regulation of vascular permeability in vivo. *Nature Communications*, *3*(1), 1–15. https://doi.org/10.1038/ncomms2199

Oshima, Y., Deering, T., Oshima, S., Nambu, H., Reddy, P. S., Kaleko, M., Connelly, S., Hackett, S. F., & Campochiaro, P. A. (2004). Angiopoietin-2 enhances retinal vessel sensitivity to vascular endothelial growth factor. *Journal of Cellular Physiology*, *199*(3), 412–417. https://doi.org/10.1002/JCP.10442

Payne, S., Val, S. De, & Neal, A. (2018). Endothelial-Specific Cre Mouse Models. *Arteriosclerosis, Thrombosis, and Vascular Biology*, *38*(11), 2550–2561. https://doi.org/10.1161/ATVBAHA.118.309669

Penn, J. S., Madan, A., Caldwell, R. B., Bartoli, M., Caldwell, R. W., & Hartnett, M. E. (2008). Vascular Endothelial Growth Factor in Eye Disease. *Progress in Retinal and Eye Research*, *27*(4), 331. https://doi.org/10.1016/J.PRETEYERES.2008.05.001

Pontes-Quero, S., Fernández-Chacón, M., Luo, W., Lunella, F. F., Casquero-Garcia, V., Garcia-Gonzalez, I., Hermoso, A., Rocha, S. F., Bansal, M., & Benedito, R. (2019). High mitogenic stimulation arrests angiogenesis. *Nature Communications*, *10*(1). https://doi.org/10.1038/S41467-019-09875-7

Prahst, C., Ashrafzadeh, P., Mead, T., Figueiredo, A., Chang, K., Richardson, D., Venkatraman, L., Richards, M., Russo, A. M., Harrington, K., Ouarne, M., Pena, A., Chen, D. F., Claesson-Welsh, L., Cho, K. S., Franco, C., & Bentley, K. (2020). Mouse retinal cell behaviour in space and time using light sheet fluorescence microscopy. *ELife*, *9*, e49779. https://doi.org/10.7554/ELIFE.49779

Radeva, M. Y., & Waschke, J. (2018). Mind the gap: mechanisms regulating the endothelial barrier. *Acta Physiologica*, *222*(1), e12860. https://doi.org/10.1111/APHA.12860

Sakuraba, J., Shintani, T., Tani, S., & Noda, M. (2013). Substrate Specificity of R3 Receptor-like Protein-tyrosine Phosphatase Subfamily toward Receptor Protein-tyrosine Kinases. *The Journal of Biological Chemistry*, *288*(32), 23421–23431. https://doi.org/10.1074/JBC.M113.458489

Sanz-Nogués, C., & O'Brien, T. (2016). In vitro models for assessing therapeutic angiogenesis. *Drug Discovery Today*, *21*(9), 1495–1503. https://doi.org/10.1016/J.DRUDIS.2016.05.016

Scott, A., & Fruttiger, M. (2009). Oxygen-induced retinopathy: a model for vascular pathology in the retina. *Eye*, *24*(3), 416–421. https://doi.org/10.1038/eye.2009.306

Shalaby, F., Rossant, J., Yamaguchi, T. P., Gertsenstein, M., Wu, X.-F., Breitman, M. L., & Schuh, A. C. (1995). Failure of blood-island formation and vasculogenesis in Flk-1-deficient mice. *Nature*, *376*(6535), 62–66. https://doi.org/10.1038/376062a0

Shen, J., Frye, M., Lee, B. L., Reinardy, J. L., McClung, J. M., Ding, K., Kojima, M., Xia, H., Seidel, C., Lima E Silva, R., Dong, A., Hackett, S. F., Wang, J., Howard, B. W., Vestweber, D., Kontos, C. D., Peters, K. G., & Campochiaro, P. A. (2014). Targeting VE-PTP activates TIE2 and stabilizes the ocular vasculature. *Journal of Clinical Investigation*, *124*(10), 4564–4576. https://doi.org/10.1172/JCI74527

Simons, M., Gordon, E., & Claesson-Welsh, L. (2016). Mechanisms and regulation of endothelial VEGF receptor signalling. *Nature Reviews Molecular Cell Biology*, *17*(10), 611–625. https://doi.org/10.1038/nrm.2016.87

Smith, L. E. H., Wesolowski, E., McLellan, A., Kostyk, S. K., D'Amato, R., Sullivan, R., & D'Amore, P. A. (1994). Oxygen-induced retinopathy in the mouse. *Investigative Ophthalmology and Visual Science*, *35*(1), 101–111. https://pubmed.ncbi.nlm.nih.gov/7507904/

Soni, D., Regmi, S. C., Wang, D.-M., DebRoy, A., Zhao, Y.-Y., Vogel, S. M., Malik, A. B., & Tiruppathi, C. (2017). Pyk2 phosphorylation of VE-PTP downstream of STIM1-induced Ca2+ entry regulates disassembly of adherens junctions. *American Journal of Physiology - Lung Cellular and Molecular Physiology*, *312*(6), L1003–L1017. https://doi.org/10.1152/AJPLUNG.00008.2017

Souma, T., Thomson, B. R., Heinen, S., Carota, I. A., Yamaguchi, S., Onay, T., Liu, P., Ghosh, A. K., Li, C., Eremina, V., Hong, Y. K., Economides, A. N., Vestweber, D., Peters, K. G., Jin, J., & Quaggina, S. E. (2018). Context-dependent functions of angiopoietin 2 are determined by the endothelial phosphatase VEPTP. *Proceedings of the National Academy of Sciences*, *115*(6), 1298–1303. https://doi.org/10.1073/pnas.1714446115

Stahl, A., Connor, K. M., Sapieha, P., Chen, J., Dennison, R. J., Krah, N. M., Seaward, M. R., Willett, K. L., Aderman, C. M., Guerin, K. I., Hua, J., Löfqvist, C., Hellström, A., & Smith, L. E. H. (2010). The Mouse Retina as an Angiogenesis Model. *Investigative Ophthalmology & Visual Science*, *51*(6), 2813–2826. https://doi.org/10.1167/IOVS.10-5176

Sternberg, N., & Hamilton, D. (1981). Bacteriophage P1 site-specific recombination: I. Recombination between loxP sites. *Journal of Molecular Biology*, *150*(4), 467–486. https://doi.org/10.1016/0022-2836(81)90375-2

Stone, J., Itin, A., Alon, T., Pe'er, J., Gnessin, H., Chan-Ling, T., & Keshet, E. (1995). Development of retinal vasculature is mediated by hypoxia-induced vascular endothelial growth factor (VEGF) expression by neuroglia. *The Journal of Neuroscience*, *15*(7 Pt 1), 4738–4747. https://doi.org/10.1523/JNEUROSCI.15-07-04738.1995

Tah, V., Orlans, H. O., Hyer, J., Casswell, E., Din, N., Sri Shanmuganathan, V., Ramskold, L., & Pasu, S. (2015). Anti-VEGF therapy and the retina: An update. *Journal of Ophthalmology*, *2015*, 627674. https://doi.org/10.1155/2015/627674

Tan, W. H., Popel, A. S., & Mac Gabhann, F. (2013). Computational Model of VEGFR2 pathway to ERK activation and modulation through receptor trafficking. *Cellular*

Signalling, *25*(12), 2496–2510. https://doi.org/10.1016/J.CELLSIG.2013.08.015

Thomson, B. R., Carota, I. A., Souma, T., Soman, S., Vestweber, D., & Quaggin, S. E. (2019). Targeting the vascular-specific phosphatase PTPRB protects against retinal ganglion cell loss in a pre-clinical model of glaucoma. *ELife*, *8*, e48474. https://doi.org/10.7554/ELIFE.48474

Tonks, N. K. (2006). Protein tyrosine phosphatases: from genes, to function, to disease. *Nature Reviews Molecular Cell Biology*, *7*(11), 833–846. https://doi.org/10.1038/nrm2039

Vähätupa, M., Järvinen, T. A. H., & Uusitalo-Järvinen, H. (2020). Exploration of Oxygen-Induced Retinopathy Model to Discover New Therapeutic Drug Targets in Retinopathies. *Frontiers in Pharmacology*, *11*, 873. https://doi.org/10.3389/FPHAR.2020.00873

Vestweber, D. (2021). Vascular endothelial protein tyrosine phosphatase regulates endothelial function. *Physiology*, *36*(2), 84–93. https://doi.org/10.1152/physiol.00026.2020

Vockel, M., & Vestweber, D. (2013). How T cells trigger the dissociation of the endothelial receptor phosphatase VE-PTP from VE-cadherin. *Blood*, *122*(14), 2512–2522. https://doi.org/10.1182/BLOOD-2013-04-499228

Wang, X., Bove, A. M., Simone, G., & Ma, B. (2020). Molecular Bases of VEGFR-2-Mediated Physiological Function and Pathological Role. *Frontiers in Cell and Developmental Biology*, *8*, 1314. https://doi.org/10.3389/FCELL.2020.599281

Wessel, F., Winderlich, M., Holm, M., Frye, M., Rivera-Galdos, R., Vockel, M., Linnepe, R., Ipe, U., Stadtmann, A., Zarbock, A., Nottebaum, A. F., & Vestweber, D. (2014). Leukocyte extravasation and vascular permeability are each controlled in vivo by different tyrosine residues of VE-cadherin. *Nature Immunology*, *15*(3), 223–230. https://doi.org/10.1038/ni.2824

Winderlich, M., Keller, L., Cagna, G., Broermann, A., Kamenyeva, O., Kiefer, F., Deutsch, U., Nottebaum, A. F., & Vestweber, D. (2009). VE-PTP controls blood vessel development by balancing Tie-2 activity. *Journal of Cell Biology*, *185*(4), 657–671. https://doi.org/10.1083/jcb.200811159

Xu, Y., & Fisher, G. J. (2012). Receptor type protein tyrosine phosphatases (RPTPs) – roles in signal transduction and human disease. *Journal of Cell Communication and Signaling*, *6*(3), 125–138. https://doi.org/10.1007/S12079-012-0171-5

Yang, D., Jin, C., Ma, H., Huang, M., Shi, G.-P., Wang, J., & Xiang, M. (2016). EphrinB2/EphB4 pathway in postnatal angiogenesis: a potential therapeutic target for ischemic cardiovascular disease. *Angiogenesis*, *19*(3), 297–309. https://doi.org/10.1007/S10456-016-9514-9

Zhang, Z.-Y. (2017). Drugging the Undruggable: Therapeutic Potential of Targeting Protein Tyrosine Phosphatases. *Accounts of Chemical Research*, *50*(1), 122–129. https://doi.org/10.1021/ACS.ACCOUNTS.6B00537

A.
APPENDIX

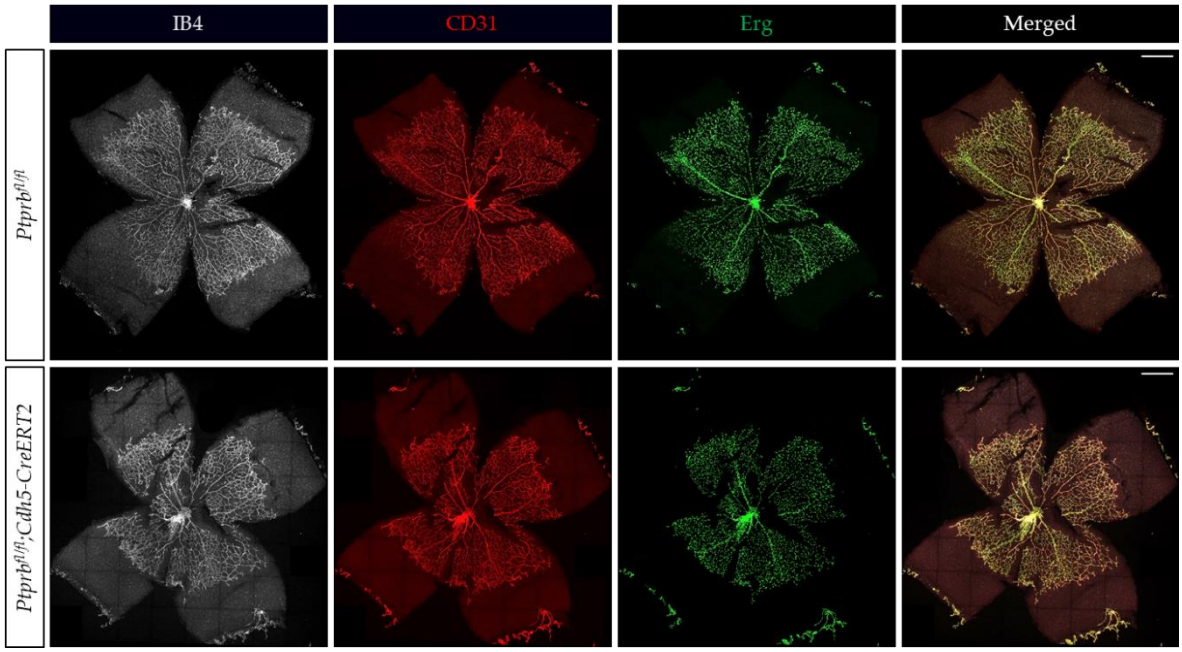

Figure 5.1. Immunostaining of P6 retinas from *Ptprb$^{fl/fl}$;Cdh5-CreERT2* or *Ptprb$^{fl/fl}$* mice. Eyes from P6 *Ptprb$^{fl/fl}$;Cdh5-CreERT2* or *Ptprb$^{fl/fl}$* pups treated at P1, P2 and P3 with 100 µg of tamoxifen were used for immunofluorescence analyses. Representative images of whole mount P6 retinas from *Ptprb$^{fl/fl}$* and *Ptprb$^{fl/fl}$;Cdh5-CreERT2* mice immunostained for CD31, IB4 and Erg. Composite of CD31 and Erg staining was used on ImageJ for tip cell density quantification. Vessel density and outgrowth from the optic nerve were quantified on ImageJ using CD31 channel. Scale bar, 500 µm.

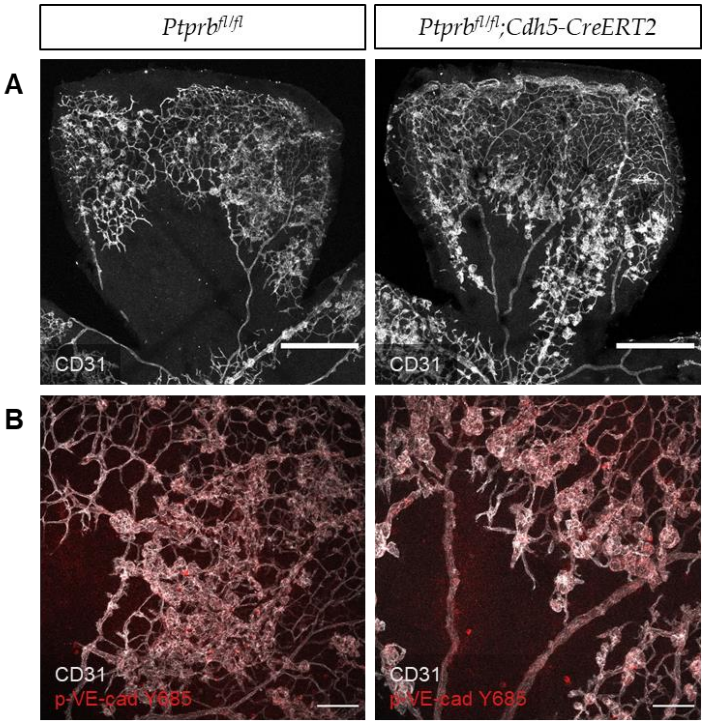

Figure 5.2. Neovascular tufts from P17 OIR mice. *Ptprb*$^{fl/fl}$*;Cdh5-CreERT2* and *Ptprb*$^{fl/fl}$ mice were submitted to OIR challenge. Pups were exposed to hyperoxia from P7 to P12. At P12 pups were returned to normoxic conditions and *Ptprb* gene deletion was induced by IP injection of 400 µg of tamoxifen at P12, P13 and P14. Eyes from P17 mice were collected and retinas were used for immunofluorescence analyses. **(A)** Representative images of whole mount retinas from *Ptprb*$^{fl/fl}$ and *Ptprb*$^{fl/fl}$*;Cdh5-CreERT2* mice, collected at P17 after OIR challenge, stained for CD31. Avascular tissue and neovascular tufts, clusters of disorganized vessels, can be observed. Scale bar, 500 µm. **(B)** Representative images of neovascular tufts from *Ptprb*$^{fl/fl}$ and *Ptprb*$^{fl/fl}$*;Cdh5-CreERT2* mice after OIR challenge, stained for CD31 and p-VE-cadherin Y685. Scale bar, 100 µm.

2021

FILIPA VIVIANA ROCHA MARTINEZ OLIVEIRA

ENDOTHELIAL CELL-SPECIFIC PHOSPHATASE VE-PTP IN REGULATION OF ENDOTHELIAL BIOLOGY

NOVA SCHOOL OF SCIENCE & TECHNOLOGY